Article

Qinlian Hongqu Decoction Modulates FXR/TGR5/GLP-1 Pathway to Improve Insulin Resistance in NAFLD Mice: Bioinformatics and Experimental Study

Published as part of ACS Omega special issue "3D Structures in Medicinal Chemistry and Chemical Biology".

Zhongyi Zhang, Yunliang He, Mei Zhao, Xin He, Zubing Zhou, Yuanyuan Yue, Tao Shen, Juncheng Liu, Gan Zhang,* and Yong Zhang*

ACCESS | Metrics & More | Article Recommendations | Supporting Information

ABSTRACT: Background: Qinglian Hongqu decoction (QLHQD), a traditional Chinese herbal remedy, shows potential in alleviating metabolic issues related to nonalcoholic fatty liver disease (NAFLD). However, its precise mode of action remains uncertain. **Objective:** This study aims to evaluate the efficacy and mechanisms of QLHQD in treating NAFLD. **Methods:** This study utilized a NAFLD mouse model to assess the effects of QLHQD on lipid metabolism, including blood lipids and hepatic steatosis, as well as glucose metabolism, including blood glucose levels, OGTT results, and serum insulin. Network pharmacology, bioinformatics, and molecular docking were used to explore how QLHQD may improve NAFLD treatment. Key proteins involved in these mechanisms were validated via WB and immunohistochemistry. Additionally, the expression of downstream pathway targets was examined to further validate the insulin resistance mechanism by which QLHQD improves NAFLD. **Results:** Animal studies demonstrated that QLHQD alleviated lipid abnormalities, hepatic steatosis, blood glucose levels, the insulin resistance index, and the OGTT results in NAFLD mice ($P < 0.05$ or 0.01). Network pharmacology and bioinformatics analyses indicated that the effects of QLHQD on NAFLD might involve bile acid secretion pathways. Subsequent validation through Western blotting, immunohistochemistry, and qPCR demonstrated that QLHQD may influence fat metabolism and insulin sensitivity in NAFLD mice via the FXR/TGR5/GLP-1 signaling pathway. **Conclusion:** QLHQD significantly alleviates glucose and lipid metabolism disorders in a high-fat diet-induced NAFLD mouse model. Its mechanism of action may involve the activation of the FXR/TGR5/GLP-1 signaling pathway in the gut, which reduces lipid accumulation and insulin resistance.
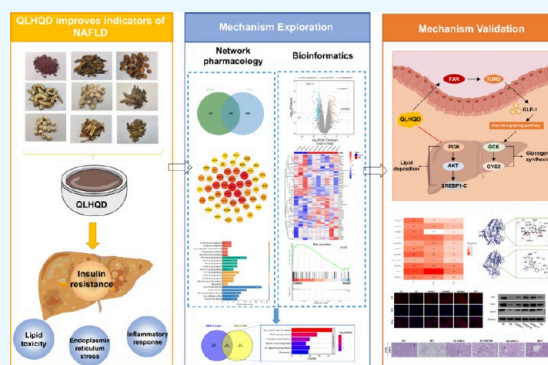
1. INTRODUCTION

Nonalcoholic fatty liver disease (NAFLD) is a clinical condition primarily characterized by diffuse hepatic steatosis.[1] There is a significant risk of progression to more severe conditions, including nonalcoholic steatohepatitis (NASH), liver fibrosis, and hepatocellular carcinoma. NAFLD is commonly seen in obese individuals and is closely linked to various systemic diseases, including metabolic syndrome, chronic kidney disease, and polycystic ovary syndrome.[2−4] Additionally, lean NAFLD is more prevalent in Asian populations, potentially due to reduced skeletal muscle mass leading to increased circulating free fatty acids, which disrupt hepatic lipid metabolism.[5] Clinically, this is often associated with the development of sarcopenia.[6,7] The current global prevalence of NAFLD is estimated to be 30%, with a rising mortality rate, thereby imposing a substantial healthcare burden in numerous countries.[8] The pathogenesis of NAFLD is primarily attributed to a "multiple hit" process, as indicated by previous studies.[9,10] The key contributing factors include overweight/obesity, type 2 diabetes, and various metabolic disorders. Insulin resistance plays a critical role in the accumulation of hepatic lipids in NAFLD.[11,12] Lifestyle modifications, including dietary restraint, adjustments in dietary structure, and increased physical activity, are considered the primary interventions for NAFLD, given the current absence of specific pharmacological treatments.[13]

Traditional Chinese Medicine (TCM) formulations, which originated from ancient practices, incorporate one or more
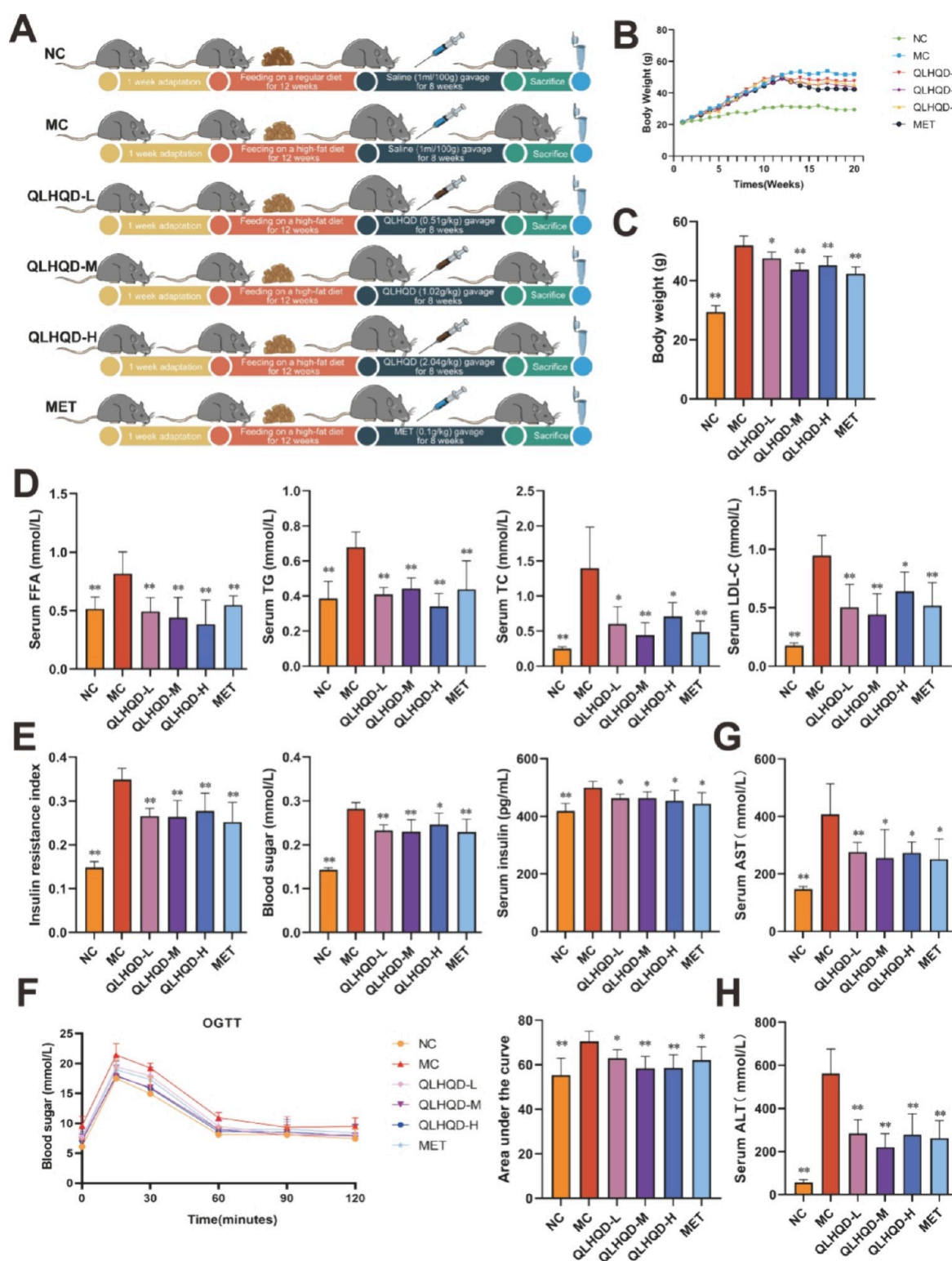
Figure 1. Impact of QLHQD on obesity and glycolipid metabolism in NAFLD mouse models. (A) Description of the animal experimental protocol. (B) Presentation of a line graph depicting mouse weight changes. (C) Analysis of body weight variations in the mice. (D) Evaluation of the influence of QLHQD on blood lipids in the NAFLD mouse model. (E) Assessment of the effects of QLHQD on blood glucose levels, insulin levels, and the insulin resistance index in the NAFLD mouse model. (F) Illustration of the oral glucose tolerance test (OGTT) curve along with the calculation of the AUC. (G,H) Impact of QLHQD on the serum AST and ALT levels in the NAFLD mouse model. Results are presented as the means ± SDs ($n = 6$). *$p < 0.05$, **$p < 0.01$, ns: not significant compared to the model control.

natural herbal remedies to address illnesses and boast a rich legacy of proven clinical effectiveness. Studies have demonstrated that TCM blends can impact diseases by targeting various pathways and mechanics.[14] Based on traditional TCM methods, the core components of the Qinlian Hongqu Decoction (QLHQD) include *Scutellaria baicalensis* Georgi.
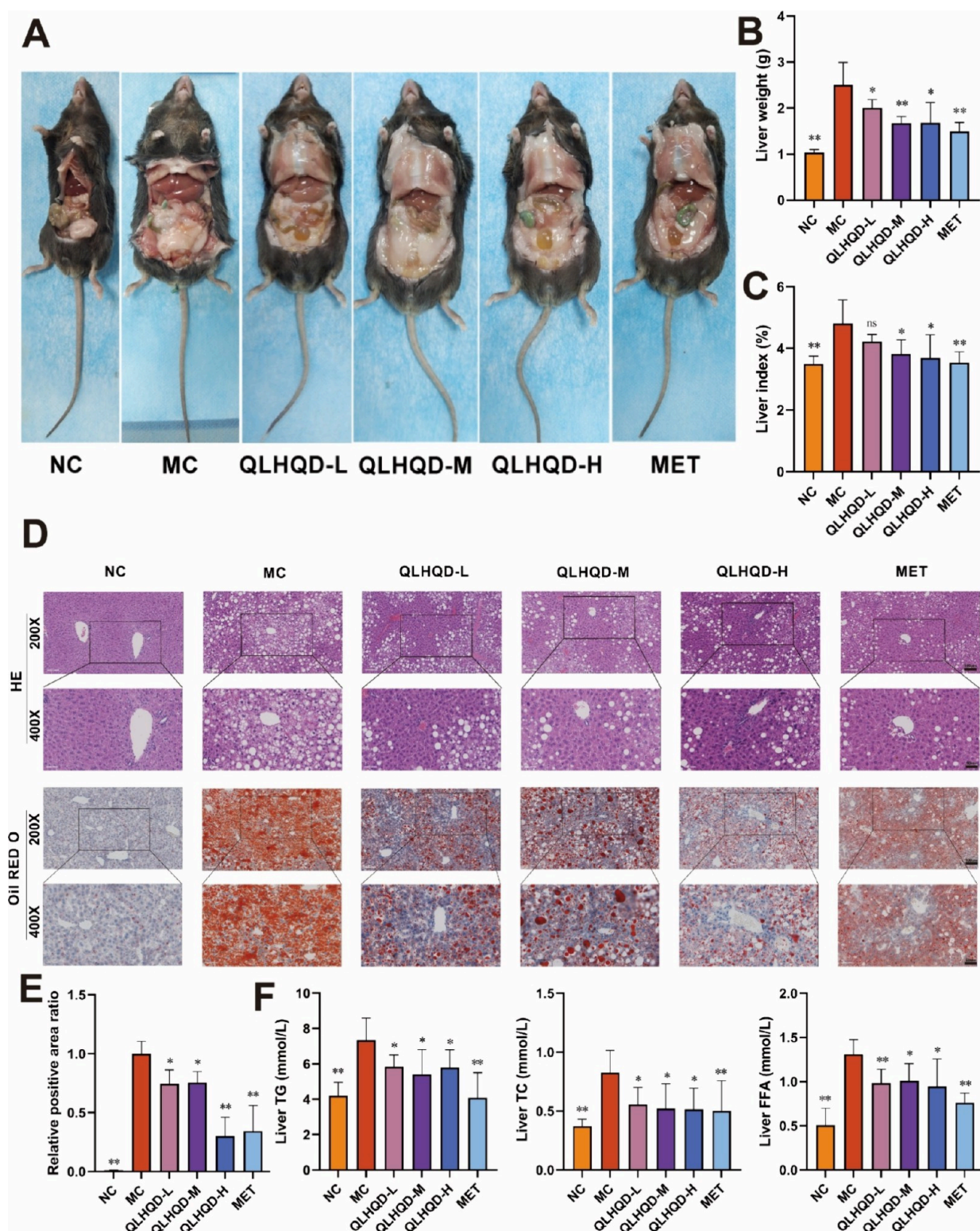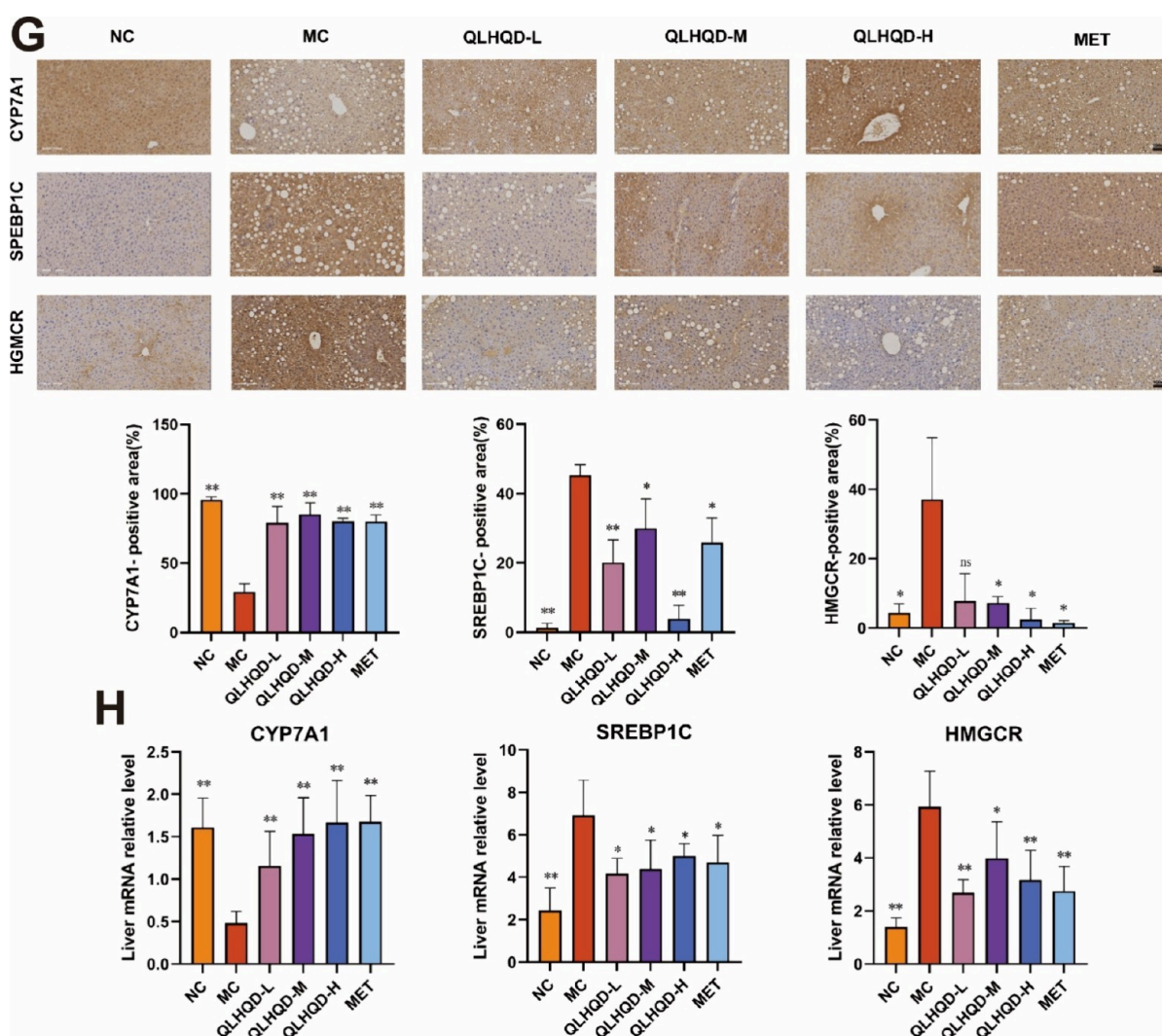
Figure 2. continued

Figure 2. Impact of QLHQD on liver lipid accumulation in NAFLD mouse models. (A) Abdominal images of each experimental group. (B) Evaluation of the influence of the QLHQDs on the liver weight of the mice, $n = 6$. (C) Assessment of the effect of QLHQD on liver weight in mice, $n = 6$. (D,E) Examination of the impact of QLHQD on histopathological alterations in the livers of NAFLD mice, $n = 3$. (F) Analysis of the effects of QLHQD on liver TG, TC, and FFA levels in NAFLD mice, $n = 6$. (G) Effects of QLHQD on the expression levels of CYP7A1, SPEBP1C, and HGMCR in NAFLD mice (×200) were examined, $n = 3$. (H) Relative mRNA levels of CYP7A1, SPEBP1C, and HGMCR were analyzed, $n = 6$. Results are presented as the means ± SDs, *$p < 0.05$, **$p < 0.01$, ns: not statistically significant compared with the model control.

(Huang Qin), *Coptis chinensis* Franch. (Huang Lian), *Monascus purpureus* Went. (Hong Qu), along with combinations of other herbs such as *Paeonia lactiflora* Pall. (Baishao), *Nelumbo nucifera* Gaertn. (Lian Zi), and *Cimicifuga heracleifolia* Kom. (Sheng Ma), roasted *Glycyrrhiza uralensis* Fisch. (Zhi Gancao), *Citrus reticulata* Blanco. (Juhong), *Citrus aurantium* L. (Zhi Qiao).[15] Preliminary studies have suggested that QLHQD may alleviate hepatic steatosis in hyperlipidemic rats.[16] Clinical reports have shown that QLHQD can improve NAFLD.[17] However, the mechanisms by which QLHQD ameliorates hepatic lipid deposition and insulin resistance in NAFLD require further investigation.

The field of network pharmacology in TCM establishes connections between drug and disease targets by utilizing database modules to investigate potential biological mechanisms.[18] Bioinformatics, which screens differential genes between patients and healthy individuals by sequencing databases, explores gene transcription and regulation and serves as a vital tool for identifying core gene targets in key diseases.[19] By integrating network pharmacology and bio-
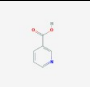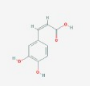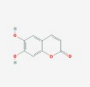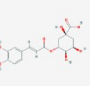
informatics, the potential mechanisms of drug interventions in diseases can be better predicted.
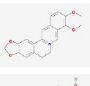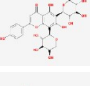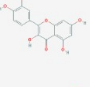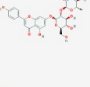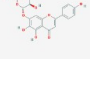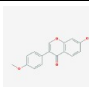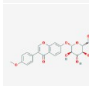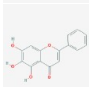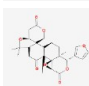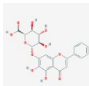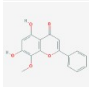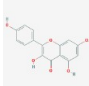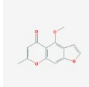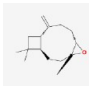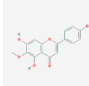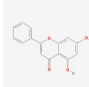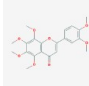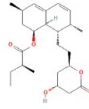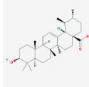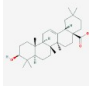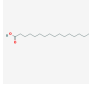
In this study, we aimed to use network pharmacology and bioinformatics to predict the potential targets of QLHQD in treating NAFLD. We also investigated the effects of QLHQD on blood lipid levels, liver lipid metabolism, and intestinal signaling pathways in high-fat diet-induced NAFLD model mice. Furthermore, we sought to understand the molecular mechanisms through which QLHQD alleviates NAFLD.

2. RESULTS

2.1. Effects of QLHQD on Obesity and Glycolipid Metabolism in NAFLD Models. Obesity, often accompanied by dyslipidemia and insulin resistance, represents a prevalent risk factor for NAFLD, resulting in disruptions in glucose and lipid metabolism. Initially, the therapeutic potential of QLHQD was investigated in NAFLD mouse models. Following 12 weeks of dietary induction, the model mice were administered QLHQD (0.51, 1.02, or 2.04 g/kg/day) or

Table 1. Core Ingredients of QLHQD

Molecule Name	ID	Structure	OB (%)	DL	Degree	Molecule Name	ID	Structure	OB (%)	DL	Degree
Nicotinic acid	MOL000421		47.64	0.02	40	Formononetin	MOL000392		69.67	0.21	50
Caffeic acid	MOL000414		54.97	0.05	56	Ononin	MOL000391		11.52	0.78	16
Esculetin	MOL003837		22.97	0.07	52	Baicalein	MOL002714		33.52	0.21	16
Chlorogenic acid	MOL001955		11.93	0.33	38	Limonin	MOL003959		21.30	0.57	76
Berberine	MOL001454		36.86	0.78	78	Baicalin	MOL002776		40.12	0.75	20
Isoliquiritigenin	MOL001789		85.32	0.15	64	Wogonin	MOL000173		30.68	0.23	84
Schaftoside	MOL007413		4.68	0.82	64	Kaempferol	MOL000422		41.88	0.24	76
Quercetin	MOL000098		46.43	0.28	74	Visnagin	MOL004029		44.25	0.15	22
Naringenin	MOL005812		6.92	0.78	90	(-)-Caryophyllene oxide	MOL002003		32.67	0.13	6
Vitexin	MOL004925		3.05	0.71	2	Hispidulin	MOL001735		30.97	0.27	88
Ferulicacid	MOL000360		39.56	0.06	78	Chrysin	MOL002560		22.61	0.18	94
Luteolin	MOL000006		36.16	0.25	78	Nobiletin	MOL005828		61.67	0.52	12
Naringin	MOL005812		6.92	0.78	20	Lovastatin	PubChem CID : 53232		-	-	6
Hesperetin	MOL002341		70.31	0.27	68	Ursolic acid	MOL000511		16.77	0.75	80
Hesperidin	MOL007930		13.33	0.67	12	Oleanolic acid	MOL000263		29.02	0.76	86
Rhoifolin	MOL000010		6.68	0.77	22	Palmitic acid	MOL000069		19.30	0.10	70
Apigenin	MOL000008		23.06	0.21	78						
Scutellarin	MOL002931		2.64	0.79	18						
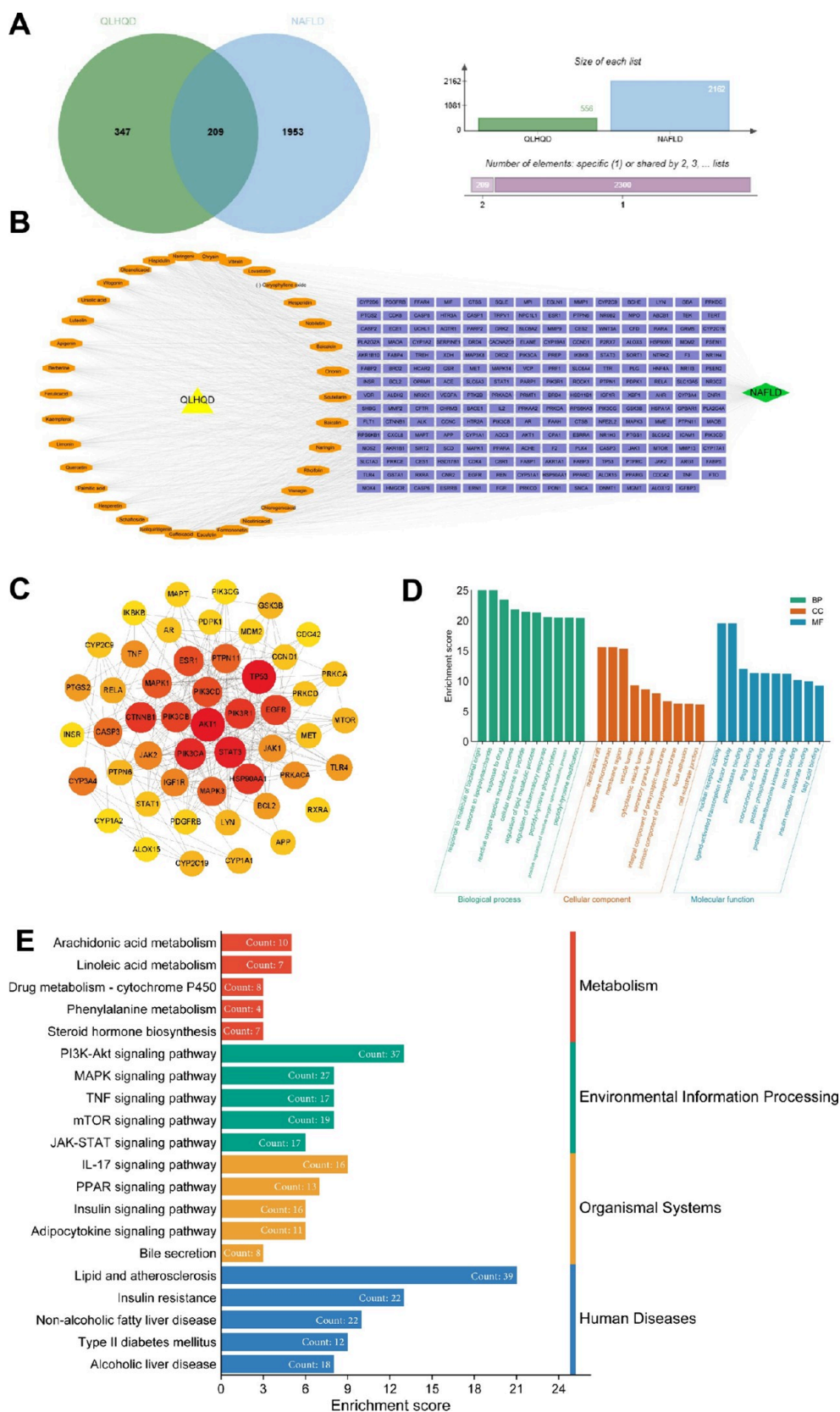
Figure 3. Network pharmacology analysis. (A) Venn diagram was used to illustrate the overlap between the QLHQD and NAFLD targets. (B) Drug-component-target-disease network was constructed, where triangles represent QLHQD, yellow nodes represent drugs for QLHQD, purple nodes represent targets, and diamond-shaped nodes represent hyperlipidemia. (C) Top 10 BPs, MFs, and CCs in the GO analysis. (D) Top 20 lipid metabolism-related pathways were determined via KEGG analysis and labeled at the pathway level. (E) Top 20 pathways related to lipid metabolism from KEGG analysis.
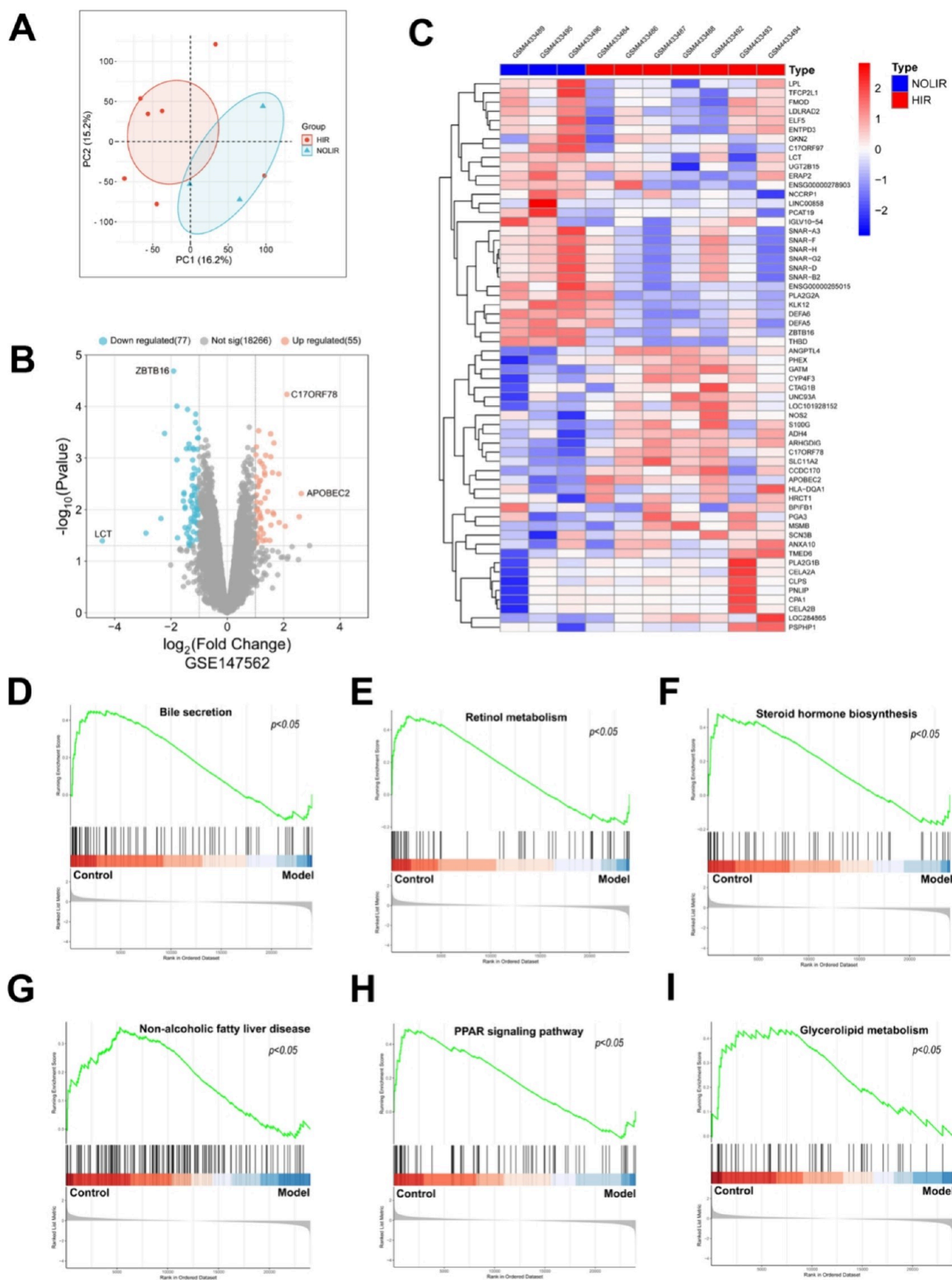
Figure 4. Bioinformatics analysis. (A) PCA of GSE147562. (B) Volcano map of DEGs in the data set. (C) Heatmap of DEGs in the data set. (D–I) GSEA results for DEGs.

metformin (0.1 g/kg/day) via gavage for an additional 8 weeks (Figure 1A). The results demonstrated that both QLHQD and metformin significantly decreased the body weight of NAFLD model mice (Figure 1B,C). The serum levels of triglycerides (TG), total cholesterol (TC), low-density lipoprotein cholesterol (LDL-C), free fatty acids (FFA), glucose, and insulin, in addition to the insulin resistance index, were assessed, and an oral glucose tolerance test (OGTT) was conducted. Compared with those in the model group, the TG, TC, LDL-C, FFA, glucose, and serum insulin levels and the insulin resistance index were notably lower in the QLHQD treatment groups (Figure 1D,E). The OGTT results indicated an increase in glucose tolerance in NAFLD mice following QLHQD treatment (Figure 1F). Furthermore, the serum levels of AST and ALT were measured, revealing a significant decrease in the QLHQD treatment groups (Figure 1G,H), suggesting that QLHQD could mitigate liver injury and inflammatory responses. In conclusion, on the basis of the analysis of blood biomarkers, QLHQD demonstrated a significant improvement in obesity and disruptions in glucose and lipid metabolism in the NAFLD mouse model.

2.2. Effects of QLHQD on Liver Lipid Deposition in NAFLD Mouse Models. Liver lipid accumulation represents a primary pathological manifestation of fatty liver disease. Hence, this study aimed to assess the impact of QLHQD on liver lipid deposition in a NAFLD mouse model induced by a high-fat diet. Following laparotomy, the liver weight was determined, and the liver index was computed. Compared with those in the model group, the liver weights and liver indices in the groups receiving QLHQD treatment were notably lower (Figure 2A−C). Histological examination of liver tissues through H&E staining revealed a significant increase in hepatocyte ballooning, lipid droplets, and hepatic inflammatory responses in the model group compared with those in the control group (Figure 2D). Similarly, Oil Red O staining revealed substantial lipid droplet accumulation in the liver tissue of the model group, whereas QLHQD and Met treatment notably ameliorated these conditions (Figure 2E,F). Furthermore, hepatic TG, TC, and FFA levels were measured via ELISA. Compared with the model group, the QLHQD treatment groups presented significantly lower levels of hepatic TG, TC, and FFA (Figure 2G), suggesting that QLHQD effectively mitigated liver lipid accumulation in NAFLD mice.

To further explore the impact of QLHQD on hepatic lipid metabolism in NAFLD mice, an analysis was conducted on the levels of the rate-limiting enzyme in the bile acid synthesis pathway (CYP7A1), the protein associated with fatty acid uptake and synthesis (SREBP1C), and the key enzyme in cholesterol synthesis (HMGCR) via immunohistochemistry (IHC). Additionally, the mRNA expression levels of these key proteins were confirmed through qRT−PCR. Compared with the model group, the group treated with QLHQD presented a notable increase in hepatic CYP7A1 expression, whereas the expression levels of SREBP1C and HMGCR decreased (Figure 2G). The mRNA expression patterns were in line with the protein expression patterns, with elevated CYP7A1 mRNA levels and reduced SREBP1C and HMGCR mRNA levels in the QLHQD treatment group (Figure 2H). These results suggest that QLHQD has the potential to regulate key proteins involved in lipid metabolism, thereby ameliorating NAFLD.

2.3. Network Pharmacology Analysis. Previous studies have identified 34 components of QLHQD through liquid chromatography−mass spectroscopy (LC−MS) and have determined their molecular structures by consulting the TCMSP and PubChem databases[16] (Table 1). The potential targets for these 34 active components were predicted via the SwissTarget Prediction and PharmMapper databases, resulting in 556 QLHQD-associated drug targets after eliminating redundancies. Potential targets for NAFLD were anticipated from the GeneCard, DisGeNET, Online Mendelian Inheritance in Man (OMIM), and Therapeutic Target Database (TTD), resulting in 2162 disease-related targets after removing duplicates. The intersection of the QLHQD drug targets and NAFLD disease targets, as depicted in a Venn diagram, revealed 209 common targets (Figure 3A). The construction of the QLHQD-NAFLD target network was accomplished via Cytoscape 3.7 (Figure 3B). Subsequently, an analysis of the 209 targets was conducted via the String database, and the top 50 genes, ranked by degree, were visualized via Cytoscape 3.7, emphasizing genes such as PI3K, AKT, and JAK, which are associated with inflammation. Notably, cytochrome P450 genes, such as CYP3A4, which are involved in bile acid synthesis, were also identified among the top 50 genes (Figure 3C). GO analysis revealed that the identified targets were enriched in 2833 biological process (BP), 263 molecular function (MF), and 127 cellular component (CC) terms. The targets for NAFLD treatment with QLHQD were enriched primarily in the following categories: BPs, including the lipopolysaccharide response, lipid metabolic process, and inflammation regulation; MFs, including fatty acid binding and insulin receptor substrate binding; and CCs, including the cytoplasmic vesicle lumen and focal adhesion (Figure 3D). Furthermore, the KEGG enrichment analysis identified 180 pathways, with common lipid metabolism-related pathways such as the PI3K-Akt signaling pathway, the MAPK signaling pathway, the PPAR signaling pathway, the TNF signaling pathway, the mTOR signaling pathway, insulin resistance, bile secretion, type II diabetes, and nonalcoholic fatty liver disease (Table S1). The top 20 lipid metabolism-related pathways were visualized on the basis of the KEGG level 1 classification (Figure 3E).

2.4. Bioinformatics Analysis. The GSE147562 data set was initially subjected to PCA via the bioinformatics platform (http://www.bioinformatics.com.cn/), which facilitated the visualization of distinct variations among samples (Figure 4A). Subsequently, differential analysis through limma identified 132 differentially expressed genes (DEGs), comprising 55 upregulated and 77 downregulated genes (Table S2). These findings are illustrated through volcano plots and heatmaps (Figure 4B,C). Furthermore, GSEA enrichment analysis of the DEGs revealed 106 significant pathways. Notably, pathways associated with lipid metabolism, such as bile acid secretion, retinol metabolism, steroid hormone biosynthesis, nonalcoholic fatty liver disease, the PPAR signaling pathway, and glycerolipid metabolism, were among those significantly downregulated in patients (Figure 4D−I).

2.5. Molecular Docking Validation. On the basis of the aforementioned research findings, the enrichment of differentially expressed genes in insulin-resistant obese individuals is linked to bile acid secretion, a pathway that is also highlighted in the KEGG enrichment analysis of QLHQD-NAFLD drug targets. Subsequent Venn diagram analysis of the KEGG enrichment pathways for TCM drug targets and GSEA results for differentially expressed genes revealed 55 common pathways. Notably, prominent pathways related to lipid
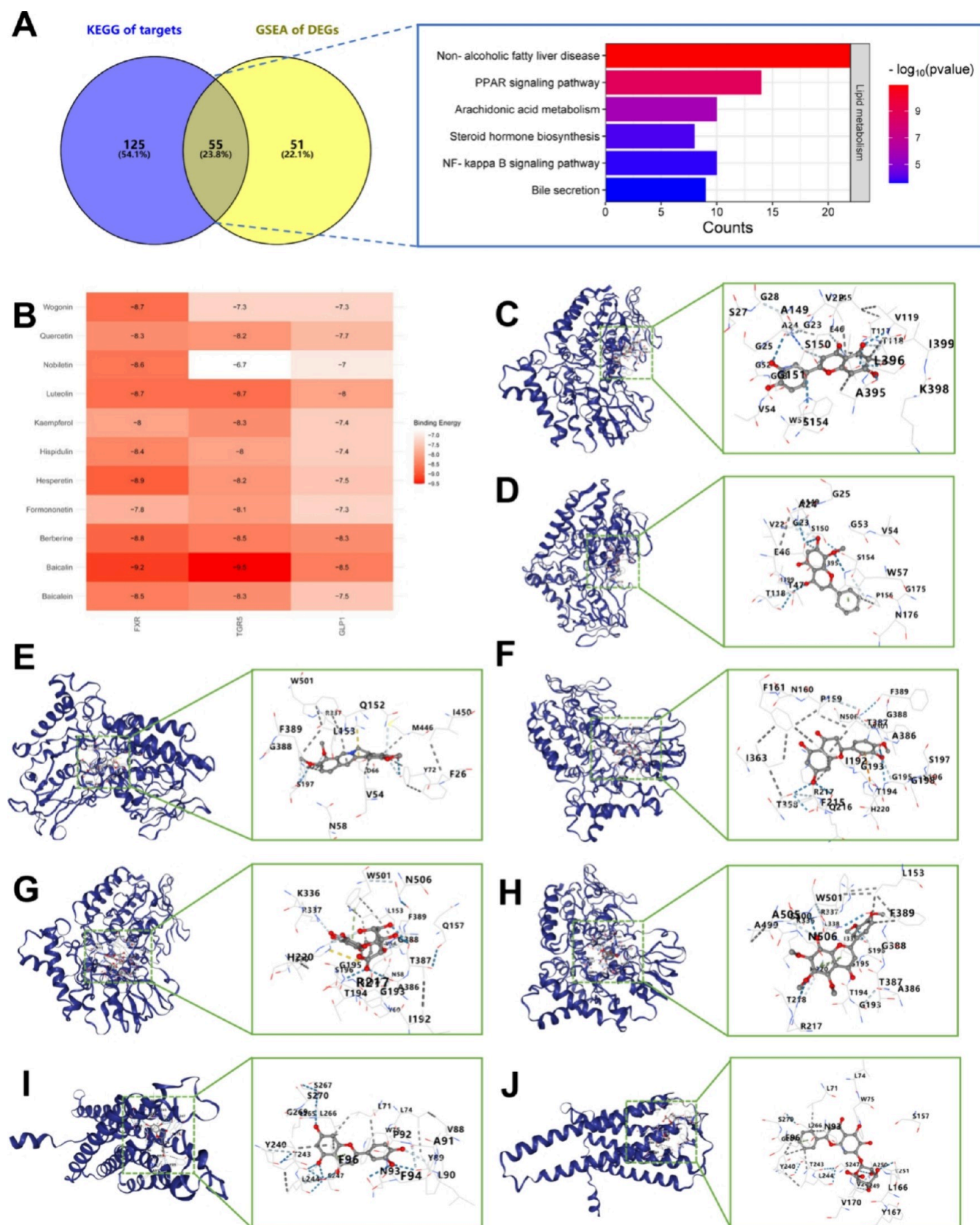
Figure 5. Validation of molecular docking. (A) Common signaling pathways identified via KEGG and GSEA. (B) Molecular docking heatmaps. (C) Binding pattern of the FXR protein with luteolin. (D) Binding mode of the FXR protein to wogonin. (E) Binding mode of the FXR protein to berberine. (F) Binding mode of the FXR protein with hesperetin. (G) Binding mode of the FXR protein with baicalin. (H) Binding mode of the FXR protein with nobiletin. (I) Binding mode of the TGR5 protein with Luteolin. (J) Binding mode of the TGR5 protein with baicalin.
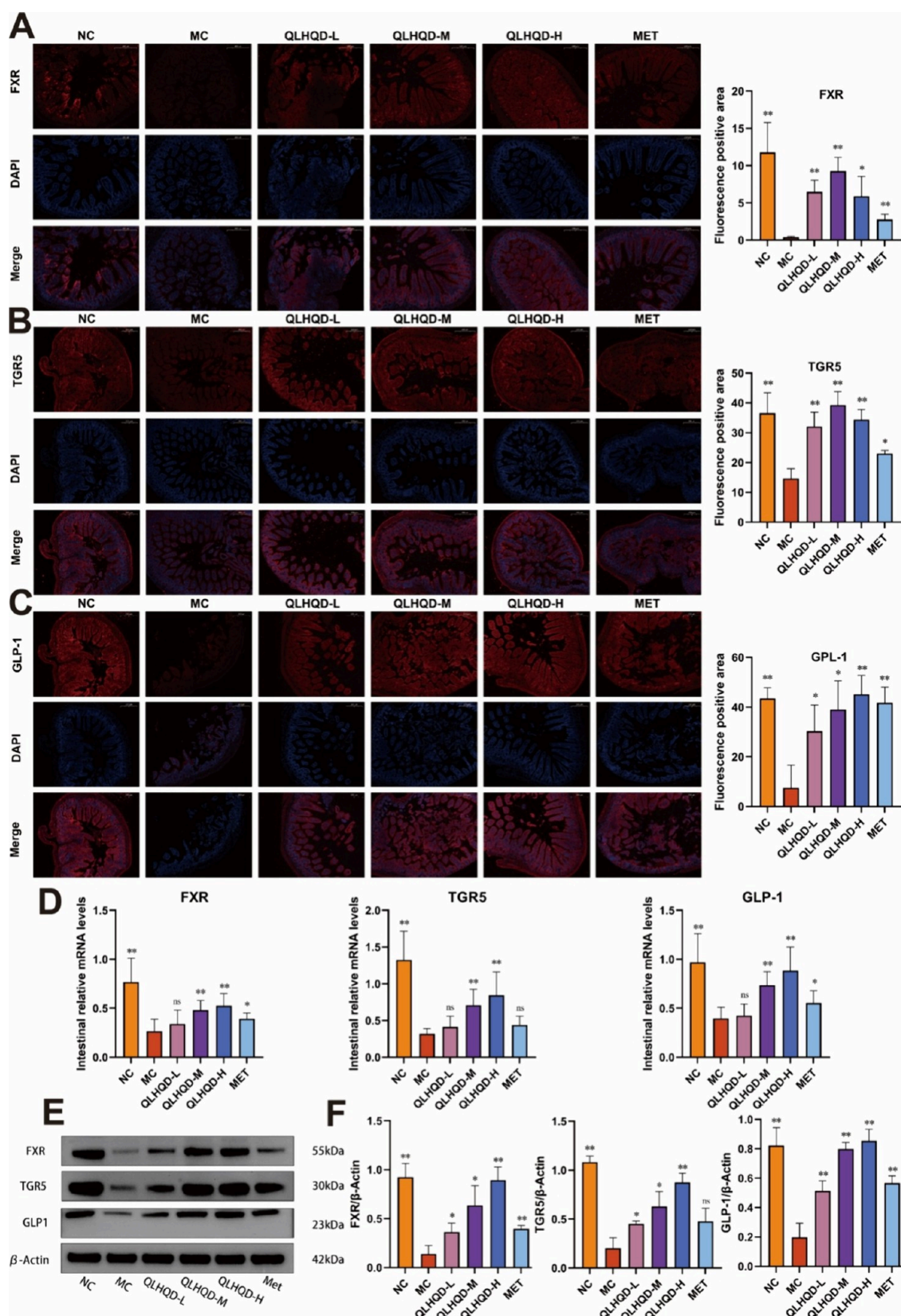
Figure 6. Impacts of QLHQD on intestinal tissue FXR, TGR5 and GLP1 in the NAFLD mouse model. (A) Identification of FXR protein expression through immunofluorescence detection (scale bar: 200 μm). (B) Identification of TGR5 protein expression through immunofluorescence detection (scale bar: 200 μm). (C) Identification of GLP1 protein expression through immunofluorescence detection (scale bar: 200 μm). (D) Relative mRNA levels of FXR, TGR5, and GLP-1, n = 6. (E) Protein expression of FXR, TGR5, and GLP-1 was detected via protein blotting. (F) Quantitative analysis of the FXR, TGR5, and GLP-1 band intensities. n = 3. Results are presented as the means ± standard deviations. Statistical significance is denoted as *$p < 0.05$, **$p < 0.01$, and ns indicates no significance compared with the model control.
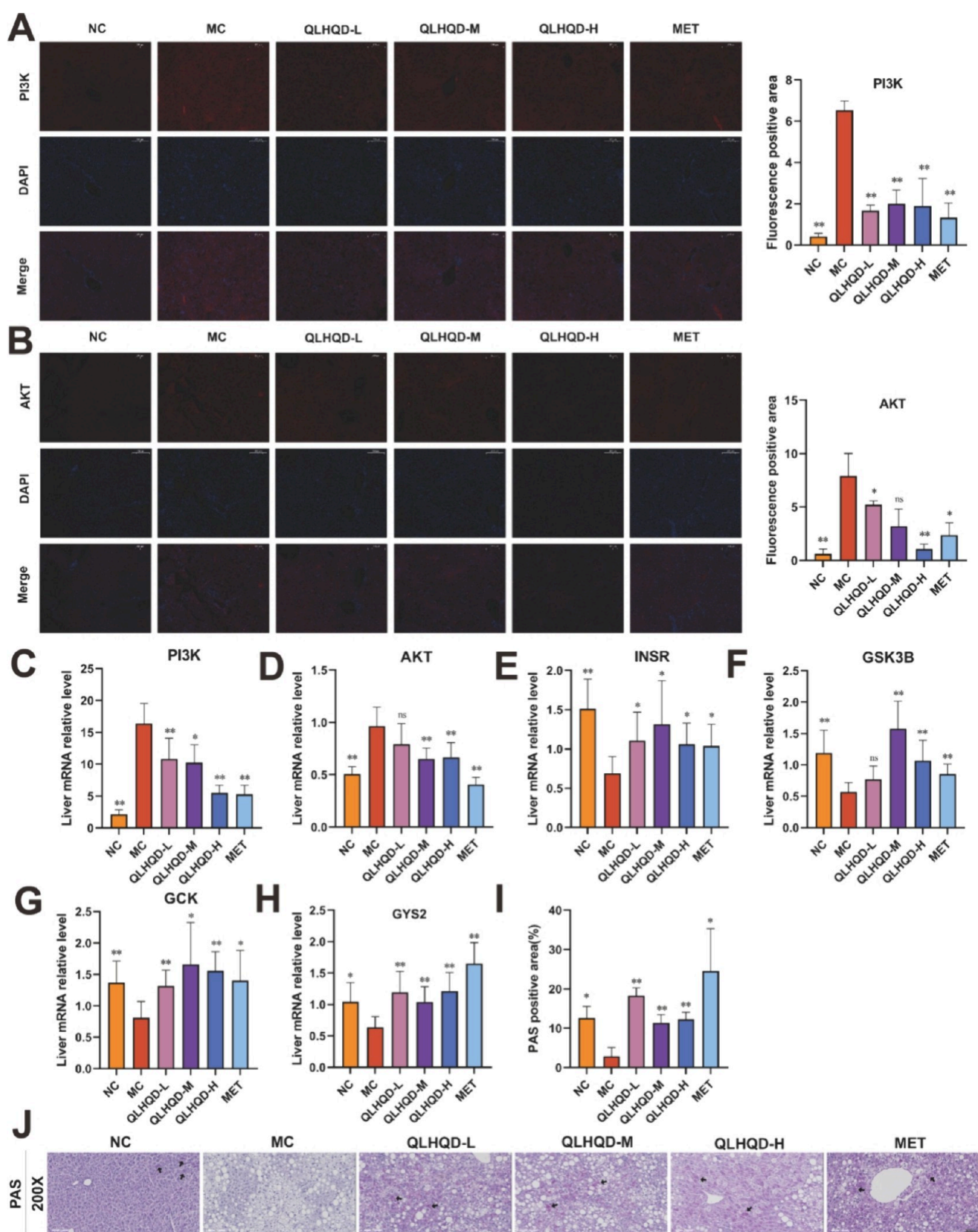
Figure 7. Effects of the QLHQDs on insulin resistance in the liver tissues of NAFLD model mice. (A) PI3K protein expression was detected via immunofluorescence (scale bar: 200 μm). (B) Identification of AKT protein expression through immunofluorescence detection (scale bar: 200 μm). (C−H) Relative mRNA levels of PI3K, AKT, INSR, GSK3B, GCk, and GYS2, $n = 6$; (I,J) PAS staining of livers and semiquantitative analysis, $n = 3$. Results are presented as the means $\pm$ standard deviations. Statistical significance is denoted as $*p < 0.05$, $**p < 0.01$, and ns indicates no significance compared with the model control.

metabolism, such as NAFLD, the PPAR signaling pathway, and bile secretion, were identified (Figure 5A). The results, in conjunction with the OGTT, serum insulin levels, and insulin resistance index data, strongly indicate that QLHQD may have a beneficial effect on NAFLD-related insulin resistance and glucose metabolism through the modulation of the intestinal bile acid metabolism pathway. Previous studies have shown that QLHQD modulates the intestinal FXR/FGF19 signaling pathway to mitigate hyperlipidemia.[20] The accumulation of cholesterol and disruptions in fatty acid metabolism are widely recognized to contribute to the exacerbation of NAFLD progression. Moreover, the literature highlights the importance of the FXR/TGR5/GLP-1 pathway as a classic bile acid metabolism pathway that directly stimulates insulin secretion.[21] Consequently, we identified 11 active components of QLHQD (Wogonin, Quercetin, Nobiletin, Luteolin, Kaempferol, Hispidulin, Hesperetin, Formononetin, Berberine, Baicalin, and Baicalein) based on the basis of their OB and DL values. Subsequently, we conducted molecular docking studies with three core targets: FXR, TGR5, and GLP-1. The findings revealed that all 11 active components presented negative binding energies with these pathway proteins (Figure 5B). Notably, the binding energies of the 11 active components with FXR were notably lower than those of the other two targets, with 8 components demonstrating binding energies below −8.5 (Figure 5C−J). This observation indicates that the primary active components of QLHQD possess robust binding affinities for FXR/TGR5/GLP-1 and have the potential to activate upstream FXR, thereby eliciting the physiological effects of the entire pathway.

2.6. Effects of QLHQD on Intestinal Tissue FXR, TGR5, and GLP-1 in NAFLD Mouse Models. Initially, immunofluorescence techniques were employed to determine the subcellular localization of the three principal targets, namely, FXR, TGR5, and GLP-1, within the intestinal tissue. The results indicated that the control cohort exhibited subdued fluorescence signals for the FXR, TGR5, and GLP-1 proteins in the small intestine, whereas the group treated with QLHQD presented a notable increase in fluorescence intensity at these specific loci (Figure 6A−C). Furthermore, qPCR analysis revealed a significant reduction in the mRNA expression levels of FXR, TGR5, and GLP-1 in the small intestines of NAFLD model mice, a trend that was effectively reversed by QLHQD treatment (Figure 6D). Subsequent WB investigations revealed substantial increases in the protein levels of FXR, TGR5, and GLP-1 in the groups treated with QLHQD and MET compared with those in the control group (Figure 6E,F). These results collectively suggest that QLHQD can activate the FXR/TGR5/GLP-1 signaling pathway.

2.7. Effects of QLHQD on Insulin Resistance in Liver Tissues of the NAFLD Mouse Models. The pivotal roles of PI3K and AKT in insulin functional biological processes are well established. Upon interaction with IRS, PI3K initiates the production of phosphoinositides, which activate AKT and subsequently phosphorylate the glycogen synthase protein GSK3B. The present investigation conducted immunofluorescence localization analysis of the PI3K and AKT proteins, demonstrating a notable increase in their fluorescence intensity in the livers of the model group. Conversely, the administration of QLHQD resulted in a reduction in their expression levels (Figure 7A,B). This observation was further supported by mRNA analysis, which revealed a similar trend for PI3K and AKT (Figure 7C,D). We also validated genes downstream of

AKT and found that the mRNA expression levels of insulin receptor (INSR), glycogen synthase kinase 3 beta (GSK3B), glucose kinase (GCK), and glycogen synthase 2 (GYS2) were significantly reduced in the model group. QLHQD notably increased these expression levels (Figure 7E−H). Additionally, liver glycogen staining confirmed that, in combination with MET treatment, QLHQD enhanced hepatic glycogen synthesis and improved metabolic disturbances (Figure 7I,J). These findings indicate that QLHQD has the potential to improve insulin resistance in NAFLD model mice.

3. DISCUSSION

This research investigates the impact of QLHQD on NAFLD by analyzing various parameters, including body weight, liver weight, serum lipid levels, blood glucose, insulin-related markers, and liver pathology, in a NAFLD mouse model. These findings indicate that QLHQD effectively enhances glucose and lipid metabolism, reduces liver lipid accumulation, and improves insulin sensitivity. To elucidate the underlying molecular mechanisms through which QLHQD ameliorates insulin resistance in NAFLD mice, network pharmacology and bioinformatics methods were utilized. By integrating these methodologies with the literature, it was discovered that QLHQD modulates the classical FXR/TGR5/GLP-1 bile acid metabolic signaling pathway, thereby mitigating insulin resistance and addressing abnormal lipid metabolism in the liver of NAFLD mice.

Prior research utilizing LC−MS technology identified 34 bioactive compounds, among which chrysin presented the highest degree value for targets associated with nonalcoholic fatty liver disease (NAFLD). This was followed by naringenin, hispidulin, oleanolic acid, wogonin, and ursolic acid. Recent investigations have shown that chrysin increases glutathione (GSH) levels and decreases malondialdehyde levels, thereby demonstrating antioxidant properties. Additionally, it influences the AMPK/mTOR/SREBP-1c signaling pathway, leading to improvements in glucose and lipid homeostasis, adipose factors, and hepatic pathology in obese rats.[22] Naringenin has been found to prevent NAFLD by modulating the NLRP3/NF-κB signaling pathway in hepatocytes.[23] Hispidulin, on the other hand, inhibits fat accumulation by downregulating the expression of PPARγ and adiponectin.[24] Oleanolic acid possesses antidiabetic and anti-inflammatory properties that alleviate chronic low-grade inflammation in liver adipose tissue by decreasing voltage-dependent anion channel expression and reactive oxygen species, inhibiting MAPK signaling, and suppressing inflammasome activation.[25] Wogonin notably decreases the serum levels of total cholesterol, triglycerides, nonesterified fatty acids, and free fatty acids, thereby enhancing myocardial lipid metabolism in high-fat diet-induced obese mice.[26] Ursolic acid effects by influencing the gut microbiota and enhancing amino acid metabolism.[27] Furthermore, research has indicated that Coptis and Monascus can enhance hepatic lipid deposition in NAFLD rats through the regulation of the PPARα signaling pathway.[28] These results underscore the advantageous impacts of the components of the QLHQD formula on hepatic lipid deposition. Expanding on these findings, our investigation revealed that QLHQD significantly diminishes serum and hepatic levels of total cholesterol, triglycerides, and free fatty acids in NAFLD mice, thereby mitigating hepatic lipid deposition and displaying a noteworthy therapeutic potential for NAFLD treatment.

By utilizing network pharmacology, this study investigated the biological processes and potential mechanisms associated with the genes shared between the targets of QLHQD and those related to NAFLD. GO enrichment analysis revealed that the treatment of NAFLD with QLHQD involves biological functions such as insulin receptor substrate binding, fatty acid binding, and regulation of the inflammatory response. The pathogenesis of NAFLD involves various factors, including insulin resistance, oxidative stress caused by excessive free radicals, and inflammation induced by reactive oxygen species in liver tissue.[29,30] The KEGG enrichment analysis also revealed significant enrichment of the insulin resistance pathway. Insulin resistance refers to impaired biological responses of target tissues, primarily liver, muscle, and adipose tissue, to insulin stimulation.[31] Many researchers now consider NAFLD a hepatic manifestation of metabolic syndrome, with insulin resistance being a major contributing factor.[32] Studies have demonstrated a negative association between whole-body and hepatic insulin sensitivity and hepatic triglyceride synthesis. During insulin resistance, hepatic glucose uptake decreases, whereas the influx of free fatty acids into the liver increases, leading to increased hepatic fat synthesis.[33] Subsequent experiments revealed that QLHQD enhances OGTT results, reduces serum insulin levels and the insulin index in NAFLD mice, and decreases the expression levels of key enzymes involved in fatty acid synthesis (SREBP1C) and cholesterol synthesis (HMGCR). The mRNA expression levels of SREBP1C and HMGCR further supported these findings. Therefore, QLHQD can ameliorate hepatic lipid accumulation in NAFLD by modulating insulin resistance.

KEGG enrichment analysis revealed that the bile secretion pathway was significantly enriched. Bile acids, which are the final products of cholesterol metabolism, play essential roles in lipid metabolism and energy balance.[34] Enterohepatic bile acid homeostasis is a crucial physiological mechanism that regulates obesity, type 2 diabetes, and NAFLD.[35] Bioinformatics utilizes omics data from extensive public databases to analyze intricate patterns and mechanisms in biological systems. In this study, gut transcriptomic data from insulin-resistant obese individuals and control cohorts were examined to detect DEGs, followed by GSEA. The findings revealed notable downregulation of genes associated with bile secretion, PPAR signaling, NAFLD, retinol metabolism, steroid hormone biosynthesis, and glycerolipid metabolism pathways in insulin-resistant obese subjects. By comparing the KEGG enrichment pathways of the TCM targets with the GSEA outcomes of the DEGs, the PPAR signaling and bile secretion pathways were identified. The experimental results revealed significant downregulation of the rate-limiting enzyme in bile acid synthesis (CYP7A1) in the NAFLD mouse model, along with increased serum and hepatic FFA levels. Recent studies suggest that disturbances in liver-gut bile acid homeostasis lead to the dysregulation of hepatic glucose and lipid metabolism, resulting in intrahepatic bile acid accumulation and inflammatory responses in NAFLD patients.[36] In conclusion, through the integration of network pharmacology, bioinformatics, mouse experiments, and literature, we propose that QLHQD may ameliorate insulin resistance and lipid accumulation in a NAFLD mouse model by modulating the bile acid secretion pathway.

The gastrointestinal tract serves as the primary location for the digestion and absorption of nutrients and plays a crucial role in maintaining the balance of glucose and lipid metabolism. The bile acid nuclear receptor FXR and the membrane receptor TGR5 are pivotal in regulating these processes.[21,37] The functions of these proteins in the intestines are closely associated with conditions such as obesity, NAFLD, and diabetes.[38] Studies have demonstrated that the specific removal of intestinal FXR leads to a reduction in TGR5 mRNA expression, resulting in the accumulation of lipids in the liver and the development of fatty liver disease. Conversely, activating FXR increases TGR5 mRNA expression, which helps reduce hepatic lipid accumulation.[39,40] GLP-1, a hormone produced by L cells in the gut, plays a role in regulating blood glucose levels by stimulating insulin release from pancreatic β-cells and inhibiting glucagon secretion from α-cells.[41] Intestinal bile acid receptor signaling influences the regulation of GLP-1, with TGR5 activation promoting GLP-1 secretion from L cells, thereby enhancing insulin release and reducing insulin resistance.[42] Previous research suggests that the FXR/TGR5/GLP-1 signaling pathway in the intestines could be a potential mechanism through which QLHQD improves lipid accumulation and insulin resistance in NAFLD. Molecular docking simulations have shown that the active components of QLHQD have a strong affinity for the FXR, TGR5, and GLP-1 proteins. Immunofluorescence experiments confirmed that QLHQD significantly increased the expression of FXR, TGR5, and GLP-1 in intestinal epithelial cells. WB results revealed a decrease in the protein expression of FXR, TGR5, and GLP-1 in the small intestine of NAFLD model mice, which was significantly improved by QLHQD. The mRNA expression of this pathway also supports these findings, suggesting that QLHQD may alleviate NAFLD by activating the FXR/TGR5/GLP-1 signaling pathway.

The molecular mechanisms responsible for insulin resistance primarily involve the activation of the insulin receptor (IR), its substrates, and kinase cascades. IRS protein phosphorylation occurs at tyrosine residues, leading to the activation of PI3K through specific domains that bind to IR. This activation generates phosphoinositides that further activate the downstream protein kinase AKT.[42] PI3K and AKT play crucial roles in hepatic insulin resistance.[43,44] Research has shown that inhibiting the PI3K/AKT signaling pathway can alleviate hepatic insulin resistance.[45] Immunofluorescence analysis revealed increased expression of PI3K and AKT in the livers of mice with NAFLD, which was significantly reversed by QLHQD treatment. The underlying mechanism of this trend has been elucidated. Insulin signaling activates AKT, which in turn increases the activity of its downstream effector mTOR and promotes the activation of the key fat synthesis transcription factor SREBP1c.[46,47] Our experiments confirmed this, with the model group showing high expression levels of SREBP1c, both via immunohistochemistry and mRNA analyses. Additionally, AKT phosphorylates various substrates, including glycogen synthase kinase-3 beta (GSK3B).[48] Our study revealed that QLHQD not only significantly reduced the mRNA expression of AKT and PI3K but also upregulated the expression of insulin receptor (INSR), glucose kinase (GCK), and glycogen synthase kinase-3 beta (GSK3B). GSK3B, a serine−threonine kinase, negatively regulates the expression of glycogen synthase 2 (GYS2).[49] Interestingly, QLHQD increased the expression of GYS2, a finding supported by liver PAS staining. This phenomenon can be explained by the fact that high blood glucose levels can regulate glycogen metabolism either dependent on or independent of insulin.[50] Glucose activates GCK, promoting the synthesis of G6P. Increased G6P directly activates GYS2, thereby stimulating

hepatic glycogen synthesis.[51,52] The elevated mRNA expression of GCK following QLHQD treatment supports this view. Consequently, the improvements in blood glucose, insulin resistance index, and OGTT results suggest that QLHQD may upregulate the FXR/TGR5/GLP-1 pathway, enhancing hepatic glycogen synthesis and counteracting insulin resistance.

Importantly, GLP-1, an incretin hormone produced by the intestine, promotes the secretion of insulin from pancreatic β-cells and inhibits the release of glucagon from α-cells, leading to increased regulation of peripheral blood glucose levels and insulin resistance.[53] In our investigation, the levels of peripheral serum insulin were greater in the model group than in the group treated with QLHQD. This difference could be attributed to two potential mechanisms. First, GLP-1, known as a glucose-dependent insulinotropic polypeptide, exhibits more significant effects on elevated blood glucose levels.[54] These findings suggest that hyperglycemia in the model group may stimulate GLP-1 more effectively, thereby improving the function of β-cells and increasing peripheral insulin levels. SecondSecond, insulin resistance involves a diminished response of target organs to insulin, often associated with impairments in insulin signaling. Studies suggest that while proximal insulin signaling remains unaffected in insulin resistance, defects in distal signaling pathways may contribute to this condition.[12,43] By enhancing insulin uptake in the liver and skeletal muscle, QLHQD may reduce hyperinsulinemia by improving distal signaling pathways in the liver.

4. CONCLUSIONS

In brief, QLHQD significantly improved glucose and lipid metabolic disorders in NAFLD model mice induced by a high-fat diet. The potential mechanism involves the activation of the intestinal FXR/TGR5/GLP-1 signaling pathway, leading to a reduction in lipid accumulation and insulin resistance. Network pharmacology, bioinformatics, and molecular docking analyses have shed light on the intricacies of the active components present in natural plant medicines. This research underscores the efficacy of QLHQD in enhancing NAFLD through the intestine−liver axis, thereby partially validating the complex interplay between liver and intestinal functions. However, due to the inherent differences between high-fat diet mouse models and human disease, caution is needed when extrapolating these results to clinical practice.[55] Subsequent investigations will leverage multiomics methodologies and cell experiments incorporating pathway modulation to delve deeper into these mechanisms.

5. METHODS AND MATERIALS

5.1. Preparation of QLHQD. The herbs used in the present study, including 10 g of *Scutellaria baicalensis* Georgi (Batch No.: 22120202, Manufacturer: Sichuan Hemuyuan Pharmaceutical Co., Ltd.), 10 g of *Coptis chinensis* Franch (Batch No.: 221001, Manufacturer: Sichuan Limin Traditional Chinese Medicine Decoction Pieces Co., Ltd.), 10 g of *Citrus reticulata* Blanco (Batch No.: 20220922, Manufacturer: Sichuan Zhongyong Pharmaceutical Co., Ltd.), 10 g of *Monascus purpureus* Went (Batch No.: 20220301, Manufacturer: Sichuan Miande Pharmaceutical Co., Ltd.), 10 g of roasted *Glycyrrhiza uralensis* Fisch (Batch No.: 211129, Manufacturer: Sichuan Heshunkang Pharmaceutical Co., Ltd.), 10 g of *Paeonia lactiflora* Pall (Batch No.: 20221024,

Manufacturer: Sichuan Zhongyong Pharmaceutical Co., Ltd.), 10 g of *Citrus aurantium* L.(Batch No.: 22080101, Manufacturer: Sichuan Zhongyong Pharmaceutical Co., Ltd.), 10 g of *Nelumbo nucifera* Gaertn. (Batch No.: 20220815, Manufacturer: Sichuan Zhongyong Pharmaceutical Co., Ltd.), and 3 g of *Cimicifuga heracleifolia* Kom. (Batch No.: 211028, Manufacturer: Sichuan Heshunkang Pharmaceutical Co., Ltd.), were sourced from Chengdu University of Traditional Chinese Medicine Affiliated Hospital. These herbs were selected on the basis of the standards outlined in the pharmacopeia of the People's Republic of China. These herbs were initially weighed and then blended for decoction. The first decoction involved soaking the mixed herbs for 20 min, followed by decoction in water at a ratio of 1:5 (g/mL). After boiling, the mixture was simmered for an additional 60 min and filtered through a double layer of gauze. For the second decoction, the herbs were decocted once more with water at a ratio of 1:2.5 (g/mL) following the same procedure. The filtrates from both decoctions were combined to reach a total volume of 600 mL and concentrated using a rotary evaporator at 60 °C for 1 h. The concentrated solution was then freeze-dried, and the resulting powder was sealed and stored at 4 °C for future use. The final freeze-dried powder had a drug concentration of 6.15 g/g.

5.2. Animals and Main Reagents. A total of seventy-two 6-week-old C57BL/6J male mice (weighing 19−20 g) were procured from SPF (Beijing) Biotechnology Co., Ltd., with the animal qualification certificate number SCXK (Beijing) 2019−0010. The animal experiment was conducted under ethics number 2022-12 and was approved by Chengdu University of Traditional Chinese Medicine. The environmental conditions included a temperature of 22 ± 1 °C, a relative humidity of 55−60%, ambient noise levels below 60 dB, a 12-h light/dark cycle, and ad libitum access to food and water. A high-fat diet (D12451, with 45 kcal% fat from total energy) and a regular diet were procured from Xiao Shu You Tai (Beijing) Biotechnology Co., Ltd. Metformin (MET) was acquired from Jiangsu Chia Tai Tianqing Pharmaceutical Co., Ltd. Reagents for lipid metabolism indicators included total cholesterol (T-CHO, catalog number 210512101) from Meikang Biotechnology Co., Ltd., triglycerides (TG, catalog number C061-a), low-density lipoproteins (LDL-C, catalog number 2021006), alanine aminotransferase (ALT, catalog number C001-a), aspartate aminotransferase (AST, catalog number C002-a), and free fatty acids (NEFAs, catalog number C123-b) from Changchun Huili Biotechnology Co., Ltd.; and insulin (INS, catalog number E-EL-M1382c) from Elabscience Biotechnology Co., Ltd. The reagents used for immunohistochemistry and fluorescence assays included AKT (Shenyang Wanlei Biotechnology Co., Ltd., batch number WL0003b), PI3K (Absin Bioscience Inc., batch number abs119725), FXR1 (ZENBIO, catalog number R26778), TGR5 (Bioss, catalog number bs-8874R), GLP1 (Bioss, catalog number bs-3796R), HMGCR (Affinity, catalog number DF6518), SREBP1 (Proteintech, catalog number 66875−1-Ig), and CYP7A1 (Affinity, catalog number DF2612).

5.3. Main Instrumentation. An automatic biochemical analyzer (BIOBASE, model: BK-200), a tissue homogenizer (Jingxin, model: Tissue-Tearor), a benchtop centrifuge (Xiangyi, model: TGL-16C), a microplate reader (BioTek, model: Epoch), a pathology microtome (Thermo Fisher Scientific (China) Co., Ltd., model: HM315), a gel imaging system (Bio-Rad, model: Chemidoc XRS+), a fluorescence

quantitative PCR instrument (Bio-Rad, model: CFX Connect), an electrophoresis apparatus (Beijing Liuyi, model: DYY-6C), an electrophoresis tank (Beijing Liuyi, model: WD-9405A), a blot transfer tank (Beijing Liuyi, model: DYCZ-40D), and a decolorization shaker (Changzhou Runhua, model: TY-80A/S) were used.

5.4. Network Pharmacology Prediction. In our prior investigation, 34 components were identified in QLHQD through the utilization of LC−MS.[16] The potential targets of these 35 active components were predicted via the SwissTargetPrediction (https://www.swisstargetprediction.ch/) and PharmMapper databases (https://lilab-ecust.cn/pharmmapper/index.html).[56] Key targets associated with NAFLD were identified through a comprehensive search across four prominent online databases: GeneCard (https://www.genecards.org/), DisGeNET (https://www.disgenet.org/), OMIM (https://www.omim.org/), and TTD (http://db.idrblab.net/ttd/). The identification of overlapping targets between QLHQD and NAFLD was accomplished utilizing Venn diagram analysis, followed by an ingredient−target network analysis. A drug−component−target−disease network was subsequently established via Cytoscape v3.7.1 to determine the multicomponent, multitarget attributes of the QLHQD in the treatment of NAFLD. Common targets were extracted through the STRING database (https://cn.string-db.org), and a protein−protein interaction (PPI) network comprising the top 50 significant genes, on the basis of degree values, was constructed and visualized via Cytoscape v3.7.1. Gene Ontology (GO) and Kyoto Encyclopedia of Genes and Genomes (KEGG) enrichment analyses of the intersecting targets were conducted and presented via the bioinformatics platform (http://www.bioinformatics.com.cn/) to elucidate the potential functions of these genes. A significance level of $p < 0.05$ was established as the threshold for the selection of relevant GO terms and KEGG pathways.[57]

5.5. Bioinformatics Analysis. To explore the association between insulin resistance and the expression of genes related to the intestine, we analyzed the GSE147562 data set obtained from the Gene Expression Omnibus (GEO) database (https://www.ncbi.nlm.nih.gov/geo). This data set consists of 14 human gut transcriptome samples, including nonobese individuals with low insulin resistance ($n = 3$) and individuals with high insulin resistance ($n = 7$), selected for comparative analysis. The analysis was performed via the Limma package in R, with differentially expressed genes (DEGs) identified on the basis of a significance threshold of p value <0.05 and $|logFC| > 1$. Visualization of DEGs was carried out through volcano plots and heatmaps generated via the Bioinformatics platform (http://www.bioinformatics.com.cn/). Furthermore, gene set enrichment analysis (GSEA) was utilized to elucidate the potential functions of the DEGs, with a focus on genes that share common biological functions, chromosomal locations, or regulatory mechanisms.[58]

5.6. Molecular Docking. Following the aforementioned analysis, molecular docking was performed to investigate the interactions between the key drug components and target proteins. The chemical structures of the drug components were sourced from the PubChem Compound database (https://pubchem.ncbi.nlm.nih.gov/). Additionally, the 3D crystal structures of the target proteins were retrieved from the PubChem database (https://pubchem.ncbi.nlm.nih.gov/). Subsequently, the PyMOL software was utilized to process and extract the target chains of the compound proteins, which were

then stored. The molecular docking procedure between the target proteins and drug molecules was executed via the cb-dock2 platform (https://cadd.labshare.cn/cb-dock2/php/blinddock.php#job_list_load).[59]

5.7. Animal Experimental Validation. *5.7.1. Model Replication.* After a one-week acclimatization period, the control group of C57BL/6J mice was provided a standard diet, whereas the remaining groups were fed a high-fat diet (D12451) to establish a model of hepatic lipid accumulation. Following a 12-week period, liver samples from four randomly chosen mice in the experimental group were obtained for histopathological analysis. The efficacy of the model was validated by the presence of fatty degeneration.

5.7.2. Drug Delivery in Groups. The mice that were successfully generated were randomly allocated to the model control group or different treatment groups through the use of a random number table, with 6 mice in each group. The QLHQD groups were subjected to high (QLHQD-H, 2.04 g/kg/d), medium (QLHQD-M, 1.02 g/kg/d), or low (QLHQD-L, 0.51 g/kg/d) doses. The conversion of human dosage to mouse dosage was based on the standard body surface area normalization method, which is commonly used for interspecies dose translation.[60] The clinical dosage of QLHQD for humans is 83 g/day, with a raw medicine concentration of 6.15 g/g, resulting in a daily dose of 13.50 g (83 g/6.15 g/g) of lyophilized powder. To convert this human dose to an equivalent mouse dose, we employed the following formula for body surface area normalization:

$$\text{Mouse dose (g/kg)} = \frac{\text{Human dose (g/day)}}{60 \text{ kg}} \times 9.1$$

Converting this human dose to the equivalent mouse dose, we calculated a high dose of 2.04 g/kg (13.50 g/60 kg * 9.1). The medium dose was set at half of the high dose (1.02 g/kg), and the low dose was half of the medium dose (0.51 g/kg). The metformin group received a dose of 0.10 g/kg. The metformin group received a dose of 0.10 g/kg. Both the blank control group and the model control group were administered an equal volume of saline via gavage. The dosage for all the groups was 10 mL/kg, which was administered once daily for 8 consecutive weeks.

5.7.3. Sample Collection and Processing. Following the final administration in this experiment, the mice underwent a 24-h fasting period while being provided unrestricted access to water. All the mice were subsequently anesthetized through an intraperitoneal injection of 0.3% pentobarbital, and blood samples were obtained from the eyeball and collected in 2 mL centrifuge tubes. The blood samples were then centrifuged at 3500 r/min for 10 min at a low temperature to separate the serum, which was subsequently transferred to EP tubes and preserved at −20 °C. A segment of fresh liver tissue was preserved in 4% paraformaldehyde, while another portion of the liver tissue was promptly inserted into precooled, labeled cryovials, rapidly frozen in liquid nitrogen, and stored at −80 °C.

5.7.4. Measurement of Body Weight, Liver Weight, and Liver Index. The body weights of the mice were assessed on a weekly basis. Subsequent to intraperitoneal anesthesia, the body weight was promptly documented. After retro-orbital blood sampling, the mice were humanely euthanized through cervical dislocation. The livers were subsequently extracted, washed with physiological saline, dried with filter paper, and

Table 2. Primers for qRT-PCR Analyses of the Relevant Sequences

target gene	FORWARD/REVERSE (F/R)	primer sequence	product length (bp)
SREBP1C	F	CAAGGCCATCGACTACATCCG	172
	R	CACCACTTCGGGGTTTCATGC	
CYP7A1	F	GCTGTGGTAGTGAGCTGTTG	78
	R	GTTGTCCAAAGGAGGTTCACC	
INSR	F	ATGGGCTTCGGGAGAGGAT	214
	R	CTTCGGGTCTGGTCTTGAACA	
GCK	F	TGAGCCGGATGCAGAAGGA	75
	R	GCAACATCTTTACACTGGCCT	
GYS2	F	CGCTCCTTGTCGGTGACATC	160
	R	CATCGGCTGTCGTTTTGGC	
PI3K	F	ACACCACGGTTTGGACTATGG	140
	R	GGCTACAGTAGTGGGCTTGG	
AKT	F	ATGAACGACGTAGCCATTGTG	116
	R	TTGTAGCCAATAAAGGTGCCAT	
GSK3β	F	ATGGCAGCAAGGTAACCACAG	193
	R	TCTCGGTTCTTAAATCGCTTGTC	
FXR	F	GGCAGAATCTGGATTTGGAATCG	101
	R	GCCCAGGTTGGAATAGTAAGACG	
TGR5	F	TGCTTCTTCCTAAGCCTACTACT	87
	R	CTGATGGTTCCGGCTCCATAG	
GLP1	F	TGAATGAAGACAAACGCCACT	92
	R	CCACTGCACAAAATCTTGGGC	

weighed. The liver index was computed utilizing the following equation: liver index = liver weight (g)/body weight (g) × 100%.

5.7.5. Oral Glucose Tolerance Tests. After an 8-week treatment period, an oral glucose tolerance test (OGTT) was conducted. Prior to the administration of glucose (2 g/kg) via gavage, all the animals were fasted for 6 h. Blood glucose concentrations were assessed at 0, 15, 30, 60, 90, and 120 min following the administration of glucose. The data obtained were graphically represented as a line graph, and the area under the curve (AUC) was computed for quantitative evaluation.

5.7.6. Biochemical Analysis and ELISA Detection. Serum levels of serum triglycerides (TG), total cholesterol (TC), low-density lipoprotein cholesterol (LDL-C), glucose, alanine aminotransferase (ALT), and aspartate aminotransferase (AST) were primarily assessed via an automated biochemical analyzer. Insulin, serum free fatty acid (FFA), and liver TC, TG, and FFA levels were determined following the protocols provided by the ELISA kits. A 200 mg liver tissue sample was homogenized in ice-cold phosphate-buffered saline (PBS) at a 1:9 (W:V) ratio in a centrifuge tube. The homogenate was then centrifuged at 12,000 r/min for 10 min at a low temperature, and the resulting supernatant was collected. Subsequently, the levels of TC, TG, and FFA in the liver tissue were quantified according to the ELISA kit instructions.

5.7.7. H&E, Oil Red, and PAS Staining. Liver tissues fixed in 4% paraformaldehyde were rinsed with distilled water and placed in 75% ethanol overnight. After dehydration, clearing, paraffin embedding, sectioning, and mounting, hematoxylin and eosin (HE) staining was performed. For Oil Red O staining, liver tissues were preinfiltrated with OCT compound, frozen, and sectioned. For PAS staining, the tissues were dehydrated through graded alcohol, immersed in 0.5% periodic acid solution, rinsed, and then stained with Schiff reagent and hematoxylin. Pathological changes in the paraffin-embedded liver sections of each mouse group were examined under a light microscope.

5.7.8. Direct Immunofluorescence Staining. Liver and small intestine paraffin sections were subjected to a series of steps for deparaffinization and rehydration. The sections were first immersed in xylene I, followed by xylene II, absolute ethanol I, absolute ethanol II, 85% ethanol, and 75% ethanol. The samples were subsequently rinsed with distilled water. The sections were then subjected to heat treatment in a citrate buffer solution (pH 6.0) via a microwave. After cooling naturally, the sections were washed three times in PBS (pH 7.4) on a decolorizing shaker for 5 min each. During the primary antibody incubation, the blocking solution was removed, and the sections were exposed to the primary antibody diluted in PBS at 4 °C overnight in a humidified chamber to prevent evaporation. Next, the sections were washed three times in PBS (pH 7.4) on a decolorizing shaker for 5 min each. After drying gently, the corresponding secondary antibody was applied, and the sections were incubated in the dark at room temperature for 50 min. DAPI staining was carried out by washing the sections three times in PBS (pH 7.4) on a decolorizing shaker for 5 min each. Subsequently, DAPI staining solution was applied, and the sections were incubated in the dark at room temperature for 10 min. The sections were then washed three more times in PBS (pH 7.4) on a decolorizing shaker for 5 min each, dried gently, and mounted with antifade medium. Finally, the slides were examined using a laser confocal microscope.

5.7.9. Real-Time Quantitative Polymerase Chain Reaction (RT-qPCR). Liver and small intestine tissues were obtained for RNA extraction using the Total RNA Miniprep Kit. Subsequently, cDNA synthesis was carried out following the manufacturer's protocol for the reverse transcription kit. Quantitative real-time PCR (RT-qPCR) was performed under the following conditions: initial denaturation at 95 °C for 5 min, followed by 40 cycles of denaturation at 95 °C for 10 s, annealing at 60 °C for 30 s, and a final melting curve analysis from 65 to 95 °C with increments of 0.5 °C every 5 s. Ct values for the target and reference genes in both the control

and experimental groups were recorded postreaction. Relative gene expression levels were calculated via the 2-ΔΔCt method. The primer sequences can be found at Table 2.

5.7.10. Immunohistochemistry. Paraffin-embedded liver tissues were sectioned and subjected to antigen retrieval using a citrate buffer (pH 6.0). The sections were incubated with a 3% hydrogen peroxide solution to inhibit endogenous peroxidase activity, followed by blocking with 3% BSA. Primary antibodies diluted in PBS were applied to the sections, which were subsequently incubated overnight at 4 °C. The sections were then treated with HRP-conjugated secondary antibodies specific to the primary antibody species. Color development was achieved via DAB, and hematoxylin was used for nuclear counterstaining. The sections were examined under a light microscope, and images were captured via a pathology slide scanner.

5.7.11. Western Blot. A 100 mg sample of small intestine tissue was homogenized in RIPA lysis buffer at a ratio of 1 mg of tissue to 10 μL of buffer and placed in a centrifuge tube. After homogenization, lysis, and centrifugation, the supernatant was collected for protein concentration determination via the BCA method. The proteins were then separated via SDS−PAGE and transferred onto a PVDF membrane at a constant voltage of 100 V. The membrane was subsequently rinsed with TBST solution containing 5% nonfat milk and blocked for 1 h. Primary antibodies were added, and the membrane was incubated overnight at 4 °C. Following rinsing, the membrane was exposed to secondary antibodies at room temperature for 1 h. After another round of washing, a chemiluminescent substrate was applied. The results were observed via a gel imaging system, with adjustments made to the exposure time, area, and background as necessary to obtain the final exposure images.

5.7.12. Statistical Analysis. All the data in this study were subjected to analysis, statistical evaluation, and graphical representation via GraphPad Prism 9.5 software. The quantitative data are presented as the means ± standard deviations ($\overline{x} + S$). For comparisons between two groups, the LSD test was used for normally distributed data; otherwise, the nonparametric Mann−Whitney U test was employed. For comparisons involving multiple groups, one-way ANOVA was conducted under the assumption of homogeneous variances; otherwise, Dunnett's T3 test was used. Statistical significance was considered at $P < 0.05$. Each experiment was repeated a minimum of three times.

■ ASSOCIATED CONTENT

Data Availability Statement

The data underlying this study are not publicly available due to laboratory confidentiality agreements and intellectual property protection. The data are available from the corresponding author upon reasonable request, subject to the establishment of a data sharing agreement.

Ⓢ Supporting Information

The Supporting Information is available free of charge at https://pubs.acs.org/doi/10.1021/acsomega.4c07463.

> Drug-disease KEGG pathway enrichment and GEO differential expression analysis data (PDF)

■ AUTHOR INFORMATION

Corresponding Authors

Gan Zhang − *Institute of Traditional Chinese Medicine, Sichuan Academy of Chinese Medicine Sciences, Chengdu 610041, China*; Email: 631071976@qq.com

Yong Zhang − *Institute of Traditional Chinese Medicine, Sichuan Academy of Chinese Medicine Sciences, Chengdu 610041, China; School of Basic Medicine, Chengdu University of Traditional Chinese Medicine, Chengdu 611137, China*; Email: 18692213920@163.com

Authors

Zhongyi Zhang − *Institute of Traditional Chinese Medicine, Sichuan Academy of Chinese Medicine Sciences, Chengdu 610041, China; School of Basic Medicine, Chengdu University of Traditional Chinese Medicine, Chengdu 611137, China;* orcid.org/0009-0001-8566-9875

Yunliang He − *Institute of Traditional Chinese Medicine, Sichuan Academy of Chinese Medicine Sciences, Chengdu 610041, China*

Mei Zhao − *School of Basic Medicine, Chengdu University of Traditional Chinese Medicine, Chengdu 611137, China*

Xin He − *School of Basic Medicine, Chengdu University of Traditional Chinese Medicine, Chengdu 611137, China; Department of Traditional Chinese Medicine, Chengdu Integrated TCM&Western Medicine Hospital, Chengdu 610041, China*

Zubing Zhou − *School of Basic Medicine, Chengdu University of Traditional Chinese Medicine, Chengdu 611137, China*

Yuanyuan Yue − *Department of Traditional Chinese Medicine, Chengdu Integrated TCM&Western Medicine Hospital, Chengdu 610041, China*

Tao Shen − *School of Basic Medicine, Chengdu University of Traditional Chinese Medicine, Chengdu 611137, China*

Juncheng Liu − *Department of Traditional Chinese Medicine, Pengzhou Hospital of Traditional Chinese Medicine, Pengzhou 611900, China*

Complete contact information is available at:
https://pubs.acs.org/10.1021/acsomega.4c07463

Author Contributions

Z.Z. and Y.H. contributed equally to this work and share first authorship. The authors confirm that all the data presented in this study were independently generated by our research team. No paper mills were utilized in the preparation of this manuscript. Z.Z.: Conceptualization, data curation, methodology, resources, visualization, writing-original draft. Y.H.: Conceptualization, data curation, formal analysis, project administration, visualization, writing—original draft, writing—review and editing. M.Z.: Data curation, formal analysis, and validation. X.H.: Data curation, software, and visualization. Z.Z.: Data curation, investigation, and validation. Y.Y.: Data curation, formal analysis. T.S.: Data curation, funding acquisition. J.L.: conceptualization, methodology, project administration. G.Z.: Conceptualization, methodology, project administration, funding acquisition. Y.Z.: Conceptualization, methodology, project administration, supervision, funding acquisition, writing—original draft, writing—review and editing.

Notes

The authors declare no competing financial interest.

The study adhered to the NC3Rs ARRIVE Guidelines. The animal experiments were reviewed and approved by the Animal Experimentation Ethics Committee of Chengdu University of Traditional Chinese Medicine on June 13, 2023, under Ethics No. 2022-11.

◼ ABBREVIATIONS

QLHQD: Qinlian hongqu Decoction
NAFLD: nonalcoholic fatty liver disease
KEGG: Kyoto-Encyclopedia of Genes and Genomes
GSEA: Gene Set Enrichment Analysis
TCM: Traditional Chinese medicine
Met: metformin
NC: nonspecific Control
MC: model control
WB: Western blot
RT−qPCR: reverse transcription-quantitative polymerase chain reaction
DEGs: differentially expressed genes

◼ REFERENCES

(1) Younossi, Z. M.; Golabi, P.; Paik, J. M.; Henry, A.; Van Dongen, C.; Henry, L. The Global Epidemiology of Nonalcoholic Fatty Liver Disease (NAFLD) and Nonalcoholic Steatohepatitis (NASH): A Systematic Review. *Hepatology* **2023**, *77* (4), 1335−1347.

(2) Takahashi, Y.; Dungubat, E.; Kusano, H.; Fukusato, T. Pathology and Pathogenesis of Metabolic Dysfunction-Associated Steatotic Liver Disease-Associated Hepatic Tumors. *Biomedicines* **2023**, *11* (10), 2761.

(3) Musso, G.; Gambino, R.; Tabibian, J. H.; Ekstedt, M.; Kechagias, S.; Hamaguchi, M.; Hultcrantz, R.; Hagström, H.; Yoon, S. K.; Charatcharoenwitthaya, P.; George, J.; Barrera, F.; Haflidadóttir, S.; Björnsson, E. S.; Armstrong, M. J.; Hopkins, L. J.; Gao, X.; Francque, S.; Verrijken, A.; Yilmaz, Y.; Lindor, K. D.; Charlton, M.; Haring, R.; Lerch, M. M.; Rettig, R.; Völzke, H.; Ryu, S.; Li, G.; Wong, L. L.; Machado, M.; Cortez-Pinto, H.; Yasui, K.; Cassader, M. Association of Non-Alcoholic Fatty Liver Disease with Chronic Kidney Disease: A Systematic Review and Meta-Analysis. *PLoS Med.* **2014**, *11*, No. e1001680.

(4) Eng, P. C.; Forlano, R.; Tan, T.; Manousou, P.; Dhillo, W. S.; Izzi-Engbeaya, C. Non-Alcoholic Fatty Liver Disease in Women - Current Knowledge and Emerging Concepts. *JHEP Rep* **2023**, *5* (10), No. 100835.

(5) Xu, R.; Pan, J.; Zhou, W.; Ji, G.; Dang, Y. Recent Advances in Lean NAFLD. *Biomed. Pharmacother.* **2022**, *153*, No. 113331.

(6) Yuan, J.; Zhang, J.; Luo, Q.; Peng, L. Effects of Nonalcoholic Fatty Liver Disease on Sarcopenia: Evidence from Genetic Methods. *Sci. Rep.* **2024**, *14* (1), 2709.

(7) Tarantino, G.; Sinatti, G.; Citro, V.; Santini, S. J.; Balsano, C. Sarcopenia, a Condition Shared by Various Diseases: Can We Alleviate or Delay the Progression? *Int. Emerg. Med.* **2023**, *18* (7), 1887−1895.

(8) Younossi, Z. M. Non-Alcoholic Fatty Liver Disease−a Global Public Health Perspective. *Journal of Hepatology* **2019**, *70* (3), 531−544.

(9) Cobbina, E.; Akhlaghi, F. Non-Alcoholic Fatty Liver Disease (NAFLD) - Pathogenesis, Classification, and Effect on Drug Metabolizing Enzymes and Transporters. *Drug Metab Rev.* **2017**, *49* (2), 197−211.

(10) Nassir, F. NAFLD: Mechanisms, Treatments, and Biomarkers. *Biomolecules* **2022**, *12* (6), 824.

(11) Fatty Liver and Alcoholic Liver Disease Group; Hepatology Branch of Chinese Medical Association; Chinese Medical Doctor Association Fatty Liver Disease Expert Committee. Guidelines for the Prevention and Treatment of Non-Alcoholic Fatty Liver Disease (2018 Update). *J. Pract. Hepatol.* **2018**, *21* (2), 177−186.

(12) Li, M.; Chi, X.; Wang, Y.; Setrerrahmane, S.; Xie, W.; Xu, H. Trends in Insulin Resistance: Insights into Mechanisms and Therapeutic Strategy. *Sig. Transduct Target Ther.* **2022**, *7* (1), 216.

(13) Eslam, M.; Sarin, S. K.; Wong, V. W.-S.; Fan, J.-G.; Kawaguchi, T.; Ahn, S. H.; Zheng, M.-H.; Shiha, G.; Yilmaz, Y.; Gani, R.; Alam, S.; Dan, Y. Y.; Kao, J.-H.; Hamid, S.; Cua, I. H.; Chan, W.-K.; Payawal, D.; Tan, S.-S.; Tanwandee, T.; Adams, L. A.; Kumar, M.; Omata, M.; George, J. The Asian Pacific Association for the Study of the Liver Clinical Practice Guidelines for the Diagnosis and Management of Metabolic Associated Fatty Liver Disease. *Hepatol Int.* **2020**, *14* (6), 889−919.

(14) Marshall, A. C. Traditional Chinese Medicine and Clinical Pharmacology. *Drug Discovery and Evaluation: Methods in Clinical Pharmacology* **2020**, *01*, 455−482.

(15) Yaqi, L.; Donghui, C.; Zhiqing, G.; Xiaobo, Z.; Juncheng, L.; Yong, Z. Clinical observation on the qinlian hongqu decoction in the adjuvant treatment of type 2 diabetes mellitus with hyperlipidemia. *Clin. J. Chin. Med.* **2023**, *15* (6), 56−59.

(16) Zhang, Y.; Guo, Z.; Wang, J.; Yue, Y.; Yang, Y.; Wen, Y.; Luo, Y.; Zhang, X. Qinlian Hongqu Decoction Ameliorates Hyperlipidemia via the IRE1-α/IKKB-β/NF-Kb Signaling Pathway: Network Pharmacology and Experimental Validation. *J. Ethnopharmacol.* **2024**, *318* (Pt A), No. 116856.

(17) Xiaobo, Z.; Yong, Z.; Shaoqian, Z.; Tao, S. Theoretical analysis and clinical application of non-alcoholic fatty liver disease based on "paste fat" theory. *J. Chengdu Univ. Trad. Chin. Med.* **2023**, *46* (1), 10−13.

(18) Zhang, P.; Zhang, D.; Zhou, W.; Wang, L.; Wang, B.; Zhang, T.; Li, S. Network Pharmacology: Towards the Artificial Intelligence-Based Precision Traditional Chinese Medicine. *Brief. Bioinform.* **2023**, *25* (1), No. bbad518.

(19) Liu, Y.; Yang, M.; Deng, Y.; Su, G.; Enninful, A.; Guo, C. C.; Tebaldi, T.; Zhang, D.; Kim, D.; Bai, Z.; Norris, E.; Pan, A.; Li, J.; Xiao, Y.; Halene, S.; Fan, R. High-Spatial-Resolution Multi-Omics Sequencing via Deterministic Barcoding in Tissue. *Cell* **2020**, *183* (6), 1665−1681.e18.

(20) Zhiqing, G.; Xiaobo, Z.; Yaqi, L.; Yang, Y.; Donghui, C.; Juncheng, L.; Yong, Z. Effects of qinlian hongqu decoction on the oxidative stress and FXR/FGF19 signaling pathway in the small intestine of hyperlipidemic rats. *Med. Pharmacol. Clin. Chin. Mater.* **2022**, *38* (6), 20−24.

(21) Jiao, N.; Baker, S. S.; Chapa-Rodriguez, A.; Liu, W.; Nugent, C. A.; Tsompana, M.; Mastrandrea, L.; Buck, M. J.; Baker, R. D.; Genco, R. J.; Zhu, R.; Zhu, L. Suppressed Hepatic Bile Acid Signalling despite

Elevated Production of Primary and Secondary Bile Acids in NAFLD. *Gut* **2018**, *67* (10), 1881−1891.

(22) Oriquat, G.; Masoud, I. M.; Kamel, M. A.; Aboudeya, H. M.; Bakir, M. B.; Shaker, S. A. The Anti-Obesity and Anti-Steatotic Effects of Chrysin in a Rat Model of Obesity Mediated through Modulating the Hepatic AMPK/mTOR/Lipogenesis Pathways. *Molecules* **2023**, *28* (4), 1734.

(23) Wang, Q.; Ou, Y.; Hu, G.; Wen, C.; Yue, S.; Chen, C.; Xu, L.; Xie, J.; Dai, H.; Xiao, H.; Zhang, Y.; Qi, R. Naringenin Attenuates Non-Alcoholic Fatty Liver Disease by down-Regulating the NLRP3/NF-κB Pathway in Mice. *Br. J. Pharmacol.* **2020**, *177* (8), 1806−1821.

(24) Lee, S. G.; Kim, J. S.; Min, K.; Kwon, T. K.; Nam, J.-O. Hispidulin Inhibits Adipogenesis in 3T3-L1 Adipocytes through PPARγ Pathway. *Chem.-biol. Interact.* **2018**, *293*, 89−93.

(25) Li, W.; Zeng, H.; Xu, M.; Huang, C.; Tao, L.; Li, J.; Zhang, T.; Chen, H.; Xia, J.; Li, C.; Li, X. Oleanolic Acid Improves Obesity-Related Inflammation and Insulin Resistance by Regulating Macrophages Activation. *Front. Pharmacol.* **2021**, *12*, No. 697483.

(26) Zhou, C.; Yin, X. Wogonin Ameliorated Obesity-Induced Lipid Metabolism Disorders and Cardiac Injury via Suppressing Pyroptosis and Deactivating IL-17 Signaling Pathway. *Am. J. Chin. Med.* **2022**, *50* (6), 1553−1564.

(27) Tian, C.; Li, J.; Bao, Y.; Gao, L.; Song, L.; Li, K.; Sun, M. Ursolic Acid Ameliorates Obesity of Mice Fed with High-Fat Diet via Alteration of Gut Microbiota and Amino Acid Metabolism. *Front. Microbiol.* **2023**, *14*, No. 1183598.

(28) Zhang, X.; Zhang, J.; Zhou, Z.; Xiong, P.; Cheng, L.; Ma, J.; Wen, Y.; Shen, T.; He, X.; Wang, L.; Zhang, Y.; Xiao, C. Integrated Network Pharmacology, Metabolomics, and Transcriptomics of Huanglian-Hongqu Herb Pair in Non-Alcoholic Fatty Liver Disease. *J. Ethnopharmacol.* **2024**, *325*, No. 117828.

(29) Fang, Y.-L.; Chen, H.; Wang, C.-L.; Liang, L. Pathogenesis of Non-Alcoholic Fatty Liver Disease in Children and Adolescence: From "Two Hit Theory" to "Multiple Hit Model. *World J. Gastroenterol.* **2018**, *24* (27), 2974−2983.

(30) Postic, C.; Girard, J. The Role of the Lipogenic Pathway in the Development of Hepatic Steatosis. *Diabetes Metab.* **2008**, *34* (6 Pt 2), 643−648.

(31) Petersen, M. C.; Shulman, G. I. Mechanisms of Insulin Action and Insulin Resistance. *Physiol. Rev.* **2018**, *98* (4), 2133−2223.

(32) James, D. E.; Stöckli, J.; Birnbaum, M. J. The Aetiology and Molecular Landscape of Insulin Resistance. *Nat. Rev. Mol. Cell Biol.* **2021**, *22* (11), 751−771.

(33) Smith, G. I.; Shankaran, M.; Yoshino, M.; Schweitzer, G. G.; Chondronikola, M.; Beals, J. W.; Okunade, A. L.; Patterson, B. W.; Nyangau, E.; Field, T.; Sirlin, C. B.; Talukdar, S.; Hellerstein, M. K.; Klein, S. Insulin Resistance Drives Hepatic de Novo Lipogenesis in Nonalcoholic Fatty Liver Disease. *J. Clin. Invest.* **2020**, *130* (3), 1453−1460.

(34) Watanabe, M.; Houten, S. M.; Mataki, C.; Christoffolete, M. A.; Kim, B. W.; Sato, H.; Messaddeq, N.; Harney, J. W.; Ezaki, O.; Kodama, T.; Schoonjans, K.; Bianco, A. C.; Auwerx, J. Bile Acids Induce Energy Expenditure by Promoting Intracellular Thyroid Hormone Activation. *Nature* **2006**, *439* (7075), 484−489.

(35) Chávez-Talavera, O.; Tailleux, A.; Lefebvre, P.; Staels, B. Bile Acid Control of Metabolism and Inflammation in Obesity, Type 2 Diabetes, Dyslipidemia, and Nonalcoholic Fatty Liver Disease. *Gastroenterology* **2017**, *152* (7), 1679−1694.e3.

(36) Tveter, K. M.; Mezhibovsky, E.; Wu, Y.; Roopchand, D. E. Bile Acid Metabolism and Signaling: Emerging Pharmacological Targets of Dietary Polyphenols. *Pharmacol. Ther.* **2023**, *248*, No. 108457.

(37) Yang, Q.; Vijayakumar, A.; Kahn, B. B. Metabolites as Regulators of Insulin Sensitivity and Metabolism. *Nature reviews. Molecular cell biology* **2018**, *19* (10), 654−672.

(38) Ma, K.; Saha, P. K.; Chan, L.; Moore, D. D. Farnesoid X Receptor Is Essential for Normal Glucose Homeostasis. *J. Clin. Invest.* **2006**, *116* (4), 1102−1109.

(39) Chiang, J. Y. L.; Ferrell, J. M. Bile Acid Receptors FXR and TGR5 Signaling in Fatty Liver Diseases and Therapy. *American Journal of Physiology. Gastrointestinal and Liver Physiology* **2020**, *318* (3), G554−G573.

(40) Pathak, P.; Xie, C.; Nichols, R. G.; Ferrell, J. M.; Boehme, S.; Krausz, K. W.; Patterson, A. D.; Gonzalez, F. J.; Chiang, J. Y. L. Intestine Farnesoid X Receptor Agonist and the Gut Microbiota Activate G-Protein Bile Acid Receptor-1 Signaling to Improve Metabolism. *Hepatology (Baltimore, Md.)* **2018**, *68* (4), 1574−1588.

(41) Abushamat, L. A.; Shah, P. A.; Eckel, R. H.; Harrison, S. A.; Barb, D. The Emerging Role of Glucagon-like Peptide-1 Receptor Agonists for the Treatment of Metabolic Dysfunction-Associated Steatohepatitis. *Clin. Gastroenterol. Hepatol.* **2024**, *22*, 1565.

(42) Yang, Y.; Tian, A.; Wu, Z.; Wei, Y.; Hu, X.; Guo, J. Finger Citron Extract Ameliorates Glycolipid Metabolism and Inflammation by Regulating GLP-1 Secretion via TGR5 Receptors in Obese Rats. *Evid.-Based Complement. Alternat. Med.* **2021**, *2021*, No. 6623379.

(43) Tonks, K. T.; Ng, Y.; Miller, S.; Coster, A. C. F.; Samocha-Bonet, D.; Iseli, T. J.; Xu, A.; Patrick, E.; Yang, J. Y. H.; Junutula, J. R.; Modrusan, Z.; Kolumam, G.; Stöckli, J.; Chisholm, D. J.; James, D. E.; Greenfield, J. R. Impaired Akt Phosphorylation in Insulin-Resistant Human Muscle Is Accompanied by Selective and Heterogeneous Downstream Defects. *Diabetologia* **2013**, *56* (4), 875−885.

(44) Alaaeldin, R.; Abdel-Rahman, I. A. M.; Hassan, H. A.; Youssef, N.; Allam, A. E.; Abdelwahab, S. F.; Zhao, Q.-L.; Fathy, M. Carpachromene Ameliorates Insulin Resistance in HepG2 Cells via Modulating IR/IRS1/PI3k/Akt/GSK3/FoxO1 Pathway. *Molecules* **2021**, *26* (24), 7629.

(45) Cheng, C.; Liu, X.-H.; He, J.; Gao, J.; Zhou, J.-T.; Fan, J.-N.; Jin, X.; Zhang, J.; Chang, L.; Xiong, Z.; Yu, J.; Li, S.; Li, X. Apolipoprotein A4 Restricts Diet-Induced Hepatic Steatosis via SREBF1-Mediated Lipogenesis and Enhances IRS-PI3K-Akt Signaling. *Mol. Nutr. Food Res.* **2022**, *66* (18), No. e2101034.

(46) Han, J.; Li, E.; Chen, L.; Zhang, Y.; Wei, F.; Liu, J.; Deng, H.; Wang, Y. The CREB Coactivator CRTC2 Controls Hepatic Lipid Metabolism by Regulating SREBP1. *Nature* **2015**, *524* (7564), 243−246.

(47) Lim, W.; Yang, C.; Bazer, F. W.; Song, G. Luteolin Inhibits Proliferation and Induces Apoptosis of Human Placental Choriocarcinoma Cells by Blocking the PI3K/AKT Pathway and Regulating Sterol Regulatory Element Binding Protein Activity1. *Biol. Reprod.* **2016**, *95* (4), 82.

(48) Saltiel, A. R. Insulin Signaling in Health and Disease. *J. Clin. Invest.* **2021**, *131* (1), No. e142241.

(49) Soto-Luna, I. C.; García-López, P. M.; Vargas-Guerrero, B.; Guzmán, T. J.; Domínguez-Rosales, J. A.; Gurrola-Díaz, C. M. Lupin Protein Isolate Improves Insulin Sensitivity and Steatohepatitis in Vivo and Modulates the Expression of the Fasn, Gys2, and Gsk3b Genes. *Food Science & Nutrition* **2021**, *9* (5), 2549−2560.

(50) Bo, T.; Gao, L.; Yao, Z.; Shao, S.; Wang, X.; Proud, C. G.; Zhao, J. Hepatic Selective Insulin Resistance at the Intersection of Insulin Signaling and Metabolic Dysfunction-Associated Steatotic Liver Disease. *Cell Metab.* **2024**, *36* (5), 947−968.

(51) Boden, G.; Chen, X.; Stein, T. P. Gluconeogenesis in Moderately and Severely Hyperglycemic Patients with Type 2 Diabetes Mellitus. *American Journal of Physiology-Endocrinology and Metabolism* **2001**, *280* (1), E23−E30.

(52) Iynedjian, P. B. Molecular Physiology of Mammalian Glucokinase. *Cell. Mol. Life Sci.* **2009**, *66* (1), 27.

(53) Li, Q.-X.; Gao, H.; Guo, Y.-X.; Wang, B.-Y.; Hua, R.; Gao, L.; Shang, H.-W.; Lu, X.; Xu, J.-D. GLP-1 and Underlying Beneficial Actions in Alzheimer's Disease, Hypertension, and NASH. *Front Endocrinol (Lausanne)* **2021**, *12*, No. 721198.

(54) Newsome, P. N.; Ambery, P. Incretins (GLP-1 Receptor Agonists and Dual/Triple Agonists) and the Liver. *J. Hepatol.* **2023**, *79* (6), 1557−1565.

(55) Zheng, Q.; Zhu, M.; Zeng, X.; Liu, W.; Fu, F.; Li, X.; Liao, G.; Lu, Y.; Chen, Y. Comparison of Animal Models for the Study of Nonalcoholic Fatty Liver Disease. *Laboratory Investigation; a Journal of Technical Methods and Pathology* **2023**, *103* (7), No. 100129.

(56) Daina, A.; Michielin, O.; Zoete, V. SwissTargetPrediction: Updated Data and New Features for Efficient Prediction of Protein Targets of Small Molecules. *Nucleic Acids Res.* **2019**, *47* (W1), W357−W364.

(57) Tang, D.; Chen, M.; Huang, X.; Zhang, G.; Zeng, L.; Zhang, G.; Wu, S.; Wang, Y. SRplot: A Free Online Platform for Data Visualization and Graphing. *PLoS One* **2023**, *18* (11), No. e0294236.

(58) Subramanian, A.; Tamayo, P.; Mootha, V. K.; Mukherjee, S.; Ebert, B. L.; Gillette, M. A.; Paulovich, A.; Pomeroy, S. L.; Golub, T. R.; Lander, E. S.; Mesirov, J. P. Gene Set Enrichment Analysis: A Knowledge-Based Approach for Interpreting Genome-Wide Expression Profiles. *Proc. Natl. Acad. Sci. U.S.A.* **2005**, *102* (43), 15545−15550.

(59) Liu, Y.; Yang, X.; Gan, J.; Chen, S.; Xiao, Z.-X.; Cao, Y. CB-Dock2: Improved Protein-Ligand Blind Docking by Integrating Cavity Detection, Docking and Homologous Template Fitting. *Nucleic Acids Res.* **2022**, *50* (W1), W159−W164.

(60) Reagan-Shaw, S.; Nihal, M.; Ahmad, N. Dose Translation from Animal to Human Studies Revisited. *Faseb J.* **2008**, *22* (3), 659−661.